

# Josephson vortices and solitons inside pancake vortex lattice in layered superconductors

A. E. Koshelev

*Materials Science Division, Argonne National Laboratory, 9700 South Cass Avenue, Argonne, IL 60439*  
(Dated: December 30, 2021)

In very anisotropic layered superconductors a tilted magnetic field generates crossing vortex lattices of pancake and Josephson vortices (JVs). We study the properties of an isolated JV in the lattice of pancake vortices. JV induces deformations in the pancake vortex crystal, which, in turn, substantially modify the JV structure. The phase field of the JV is composed of two types of phase deformations: the regular phase and vortex phase. The phase deformations with smaller stiffness dominate. The contribution from the vortex phase smoothly takes over with increasing magnetic field. We find that the structure of the cores experiences a smooth yet qualitative evolution with decrease of the anisotropy. At large anisotropies pancakes have only small deformations with respect to position of the ideal crystal while at smaller anisotropies the pancake stacks in the central row smoothly transfer between the neighboring lattice positions forming a solitonlike structure. We also find that even at high anisotropies pancake vortices strongly pin JVs and strongly increase their viscous friction.

PACS numbers: 74.25.Qt, 74.25.Op, 74.20.De,

## I. INTRODUCTION

The vortex state in layered superconductors has a very rich phase diagram in the multidimensional space of temperature-field-anisotropy-field orientation. Especially interesting subject is the vortex phases in layered superconductors with very high anisotropy such as  $\text{Bi}_2\text{Sr}_2\text{CaCu}_2\text{O}_x$  (BSCCO). Relatively simple vortex structures are formed when magnetic field is applied along one of the principal axes of the layered structure. A magnetic field applied perpendicular to the layers penetrates inside the superconductor in the form of pancake vortices (PVs).<sup>1</sup> PVs in different layers are coupled weakly via the Josephson and magnetic interactions and form aligned stacks at low fields and temperatures (PV stacks). These stacks are disintegrated at the melting point. In another simple case of the magnetic field applied parallel to the layers the vortex structure is completely different. Such a field penetrates inside the superconductor in the form of Josephson vortices (JVs).<sup>2,3,4</sup> The JVs do not have normal cores, but have rather wide nonlinear cores, of the order of the Josephson length, located between two central layers. At small in-plane fields JVs form the triangular lattice, strongly stretched along the direction of the layers, so that JVs form stacks aligned along the  $c$  direction and separated by a large distance in the in-plane direction.

A rich variety of vortex structures were theoretically predicted for the case of tilted magnetic field, such as the kinked lattice,<sup>4,5,7</sup> tilted vortex chains<sup>8</sup>, coexisting lattices with different orientation.<sup>9</sup> A very special situation exists in highly anisotropic superconductors, in which the magnetic coupling between the pancake vortices in different layers is stronger than the Josephson coupling. In such superconductors a tilted magnetic field creates a unique vortex state consisting of two qualitatively different interpenetrating sublattices.<sup>5,6</sup> This set of crossing

lattices (or combined lattice<sup>5</sup>) contains a sublattice of Josephson vortices generated by the component of the field parallel to the layers, coexisting with a sublattice of stacks of pancake vortices generated by the component of the field perpendicular to the layers. A basic reason for such an exotic ground state, as opposed to a simple tilted vortex lattice, is that magnetic coupling energy is minimal when pancake stacks are perfectly aligned along the  $c$  axis. A homogeneous tilt of pancake lattice costs too much magnetic coupling energy, while formation of Josephson vortices only weakly disturbs the alignment of pancake stacks.

Even at high anisotropies JVs and pancake stacks have significant attractive coupling.<sup>6</sup> The strong mutual interaction between the two sublattices leads to a very rich phase diagram with many nontrivial lattice structures separated by phase transitions. At sufficiently small  $c$ -axis fields (10-50 gauss) a phase separated state is formed: density of the pancake stacks located at JVs becomes larger than the stack density outside JVs.<sup>6,14</sup> This leads to formation of dense stack chains separated by regions of dilute triangular lattice in between (mixed chain+lattice state). Such structures have been observed in early decoration experiments<sup>15,16</sup> and, more recently, by scanning Hall probe<sup>17</sup>, Lorentz microscopy<sup>18</sup>, and magnetooptical technique.<sup>19,20</sup> At very small  $c$ -axis fields ( $\sim$  several gauss) the regions of triangular lattice vanish leaving only chains of stacks.<sup>17</sup> Moreover, there are experimental indications<sup>17</sup> and theoretical reasoning<sup>21</sup> in favor of the phase transition from the crossing configuration of pancake-stack chains and JVs into chains of tilted vortices. JVs also modify the interaction between pancake stacks leading to an attractive interaction between the stacks at large distances.<sup>22</sup> As a consequence, one can expect clustering of the pancake stacks at small concentrations.

Many unexpected observable effects can be naturally

interpreted within the crossing lattices picture. The underlying JV lattice modifies the free energy of the vortex crystal state. An observable consequence of this change is a shift of the melting temperature. Strong support for the crossing-lattices ground state is the linear dependence of the  $c$ -axis melting field on the in-plane field observed within a finite range of in-plane fields.<sup>6,12,13,23,24</sup> In an extended field range several melting regimes have been observed<sup>23,24</sup> indicating several distinct ground states of vortex matter in tilted fields. Transitions between different ground state configurations have also been detected by the features in the irreversible magnetization.<sup>25,26</sup>

In this paper we consider in detail the properties of an isolated JV in the pancake lattice. We mainly focus on the regime of a dense pancake lattice, when many rows of the pancakes fit into the JV core. The pancake lattice forms an effective medium for JVs which determines their properties. The dense pancake lattice substantially modifies the JV structure. In general, the phase field of the JV is built up from the continuous regular phase and the phase perturbations created by pancake displacements. Such a JV has a smaller core size and smaller energy as compared to the ordinary JV.<sup>6</sup> The pancake lattice also strongly modifies the field and current distribution far away from the core region.<sup>11</sup>

The key parameter which determines the structure of the JV core in the dense pancake lattice is the ratio  $\alpha = \lambda/\gamma s$ , where  $\lambda$  is the in-plane London penetration depth,  $\gamma$  is the anisotropy ratio, and  $s$  is the period of layered structure. The core structure experiences a smooth yet qualitative evolution with decrease of this parameter. When  $\alpha$  is small (large anisotropies) pancakes have only small displacements with respect to positions of the ideal crystal and the JV core occupies several pancakes rows. In this situation the renormalization of the JV core by the pancake vortices can be described in terms of the continuous vortex phase which is characterized by its own phase stiffness (effective phase stiffness approach).<sup>6</sup> At large  $\alpha$  (small anisotropies) the core shrinks to scales smaller than the distance between pancake vortices. In this case pancake stacks in the central row form soliton-like structure smoothly transferring between the neighboring lattice position.

We consider dynamic properties of JVs in the case of small  $\alpha$ : the critical pinning force which sticks the JV to the PV lattice and the viscosity of the moving JV due to the traveling displacement field in the PV lattice. The pinning force has a nonmonotonic dependence on the  $c$ -axis magnetic field,  $B_z$ , reaching maximum when roughly one pancake row fits inside the JV core region. At higher fields the pinning force decays exponentially  $\propto \exp(-\sqrt{B_z/B_0})$ . We study JV motion through the PV lattice and find that the lattice strongly hinders the mobility of JVs.

The paper is organized as follows. Section II is devoted to the static structure of an isolated JV inside the PV lattice. In this section we

- consider small  $c$ -axis fields and calculate the cross-

ing energy of JV and PV stack (IIB);

- consider large  $c$ -axis fields and introduce the “effective phase stiffness” approximation, which allows for simple description of JV structure inside the dense PV lattice in the case of large anisotropy (IIC);
- investigate a large-scale behavior and JV magnetic field (IID);
- analyze the JV core quantitatively using numeric minimization of the total energy and find crossover from the JV core structure to the soliton core structure with decrease of anisotropy (IIE);
- formulate a simple model which describes the soliton core structure for small anisotropies (IIF).

In Section III we consider pinning of JV by the pancake lattice and calculate the field dependence of the critical current at which the JV detaches from the PV lattice. In Section IV we consider possible JV dynamic regimes: dragging the pancake lattice by JVs and motion of JVs through the pancake lattice. For the second case we calculate the effective JV viscosity.

## II. STRUCTURE AND ENERGY OF JOSEPHSON VORTEX IN PANCAKE LATTICE

### A. General relations

Our calculations are based on the Lawrence-Doniach free energy in the London approximation, which depends on the in-plane phases  $\phi_n(\mathbf{r})$  and vector-potential  $\mathbf{A}(\mathbf{r})$

$$F = \sum_n \int d^2\mathbf{r} \left[ \frac{J}{2} \left( \nabla_\perp \phi_n - \frac{2\pi}{\Phi_0} \mathbf{A}_\perp \right)^2 + E_J \left( 1 - \cos \left( \phi_{n+1} - \phi_n - \frac{2\pi s}{\Phi_0} A_z \right) \right) \right] + \int d^3\mathbf{r} \frac{\mathbf{B}^2}{8\pi}, \quad (1)$$

where

$$J \equiv \frac{s\Phi_0^2}{\pi(4\pi\lambda)^2} \equiv \frac{s\varepsilon_0}{\pi} \text{ and } E_J \equiv \frac{\Phi_0^2}{s\pi(4\pi\lambda_c)^2} \quad (2)$$

are the phase stiffness and the Josephson coupling energy,  $\lambda \equiv \lambda_{ab}$  and  $\lambda_c$  are the components of the London penetration depth and  $s$  is the interlayer periodicity. We use the London gauge,  $\text{div} \mathbf{A} = 0$ . We assume that the average magnetic induction  $\mathbf{B}$  inside the superconductor is fixed.<sup>10</sup> The  $c$  component of the field fixes the concentration of the pancake vortices  $n_v \equiv B_z/\Phi_0$  inside one layer. The in-plane phases  $\phi_n$  have singularities at the positions of pancake vortices  $\mathbf{R}_{in}$  inside the layers,

$$[\nabla \times \nabla \phi_n]_z = 2\pi \sum_i \delta(\mathbf{r} - \mathbf{R}_{in}).$$

The major obstacle, preventing a full analytical consideration of the problem, is the nonlinearity coming from the Josephson term. A useful approach for superconductors with weak Josephson coupling is to split the phase and vector-potential into the vortex and regular contributions,  $\phi_n = \phi_{vn} + \phi_{rn}$  and  $\mathbf{A} = \mathbf{A}_v + \mathbf{A}_r$ . The vortex contributions minimize the energy for fixed positions of pancake vortices at  $E_J = 0$  and give magnetic interaction energy for the pancake vortices. One can express this part of energy via the vortex coordinates  $\mathbf{R}_{n,i}$ . In gen-

eral, the regular contributions may include phases and vector-potentials of the Josephson vortices. The total energy naturally splits into the regular part  $F_r$ , the energy of magnetic interactions between pancakes  $F_M$ , and the Josephson energy  $F_J$ , which couples the regular and vortex degrees of freedom,

$$F = F_r + F_M + F_J \quad (3)$$

with

$$F_r[\phi_{rn}, \mathbf{A}_r] = \sum_n \int d^2\mathbf{r} \frac{J}{2} \left( \nabla \phi_{rn} - \frac{2\pi}{\Phi_0} \mathbf{A}_{r\perp} \right)^2 + \int d^3\mathbf{r} \frac{\mathbf{B}_r^2}{8\pi}, \quad (4)$$

$$F_M[\mathbf{R}_{n,i}] = \frac{1}{2} \sum_{n,m,i,j} U_M(\mathbf{R}_{n,i} - \mathbf{R}_{m,j}, n - m), \quad (5)$$

$$F_J[\phi_{rn}, \mathbf{A}_r, \mathbf{R}_{n,i}] = \sum_n \int d^2\mathbf{r} E_J \left( 1 - \cos \left( \phi_{n+1} - \phi_n - \frac{2\pi s}{\Phi_0} A_z \right) \right), \quad (6)$$

and

$$U_M(\mathbf{R}, n) = \frac{J}{2\pi} \int d\mathbf{k} \int_{-\pi}^{\pi} dq \frac{\exp[i\mathbf{k}\mathbf{R} + iqn]}{k^2 [1 + \lambda^{-2}(k^2 + 2(1 - \cos q)/s^2)^{-1}]} \\ \approx 2\pi J \left[ \ln \frac{L}{R} \left[ \delta_n - \frac{s}{2\lambda} \exp \left( -\frac{s|n|}{\lambda} \right) \right] + \frac{s}{4\lambda} u \left( \frac{r}{\lambda}, \frac{s|n|}{\lambda} \right) \right] \quad (7)$$

is the magnetic interaction between pancakes<sup>1</sup> where

$$u(r, z) \equiv \exp(-z)E_1(r - z) + \exp(z)E_1(r + z), \quad (8)$$

$E_1(u) = \int_u^\infty (\exp(-v)/v) dv$  is the integral exponent ( $E_1(u) \approx -\gamma_E - \ln u + u$  at  $u \ll 1$  with  $\gamma_E \approx 0.577$ ),  $r \equiv \sqrt{R^2 + (ns)^2}$ , and  $L$  is a cutoff length.

In this paper we focus on the crystal state. If the pancake coordinates have only small deviations from the positions  $\mathbf{R}_i^{(0)}$  of the ideal triangular lattice,  $\mathbf{R}_{ni} = \mathbf{R}_i^{(0)} + \mathbf{u}_{ni}$  then  $F_v$  reduces to the energy of an ideal crystal  $F_{cr}$  plus the magnetic elastic energy  $F_{M-el}$  consisting of the shear and compression parts,

$$F_{M-el} = \int \frac{d^3\mathbf{k}}{(2\pi)^3} \left[ \frac{U_t(\mathbf{k})}{2} |u_t(\mathbf{k})|^2 + \frac{U_l(\mathbf{k})}{2} |u_l(\mathbf{k})|^2 \right], \quad (9)$$

where

$$\mathbf{u}_{ni} \equiv \int \frac{d^3\mathbf{k}}{(2\pi)^3} \exp \left( i\mathbf{k}_\perp \mathbf{R}_i^{(0)} + ik_z sn \right) [\mathbf{e}_t u_t(\mathbf{k}) + \mathbf{e}_l u_l(\mathbf{k})]$$

( $\mathbf{e}_l$  ( $\mathbf{e}_t$ ) is the unit vector parallel (orthogonal) to  $\mathbf{k}_\perp$ ),

$$U_t(\mathbf{k}) = C_{66}k_\perp^2 + U_{44}(\mathbf{k}), \\ U_l(\mathbf{k}) = U_{11}(\mathbf{k}) + U_{44}(\mathbf{k}),$$

$U_{11}$  is the compression stiffness,  $C_{66}$  is the shear modulus. In particular, at high fields,  $B_z \gg \Phi_0/\lambda^2$ , we have

$$U_{11} \equiv C_{11}(\mathbf{k})k_\perp^2 \approx \frac{B_z^2}{4\pi\lambda^2} \left( 1 - \frac{k_\perp^2}{16\pi n_v} \right), \\ C_{66} = n_v \epsilon_0 / 4$$

The magnetic tilt stiffness,<sup>29</sup>  $U_{44}(\mathbf{k})$ , is given by interpolation formula, which takes into account softening due to pancake fluctuations,

$$U_{44}(\mathbf{k}) \equiv C_{44}(k_z)k_z^2 \\ = \frac{B_z \Phi_0}{2(4\pi)^2 \lambda^4} \ln \left( 1 + \frac{r_{cut}^2}{k_z^{-2} + r_w^2} \right) \quad (10)$$

with  $r_w^2 = \langle (u_{n+1} - u_n)^2 \rangle$ ,  $r_{cut} \approx \lambda$  at  $a > \lambda$  and  $r_{cut} \approx a/4.5$  at  $a < \lambda$ ,<sup>27</sup> with  $a = \sqrt{2/(\sqrt{3}n_v)}$  being the lattice constant. At finite Josephson energy minimization of the energy with respect to the phases at fixed pancake positions leads to the Josephson term in the tilt stiffness energy.<sup>30</sup>

The major focus of this paper is the structure of JV core. This requires analysis of the pancake displacements and regular phase at distances  $r_\perp \ll \lambda_c$  and  $z \ll a, \lambda$  from the vortex center. At these distances the main contribution to the energy is coming from the kinetic en-

ergy of supercurrents and magnetic screening can be neglected. The structure of energy is significantly simplified:

$$F_r[\phi_{rn}, \mathbf{A}_r] \rightarrow F_r[\phi_{rn}] = \sum_n \int d^2\mathbf{r} \frac{J}{2} (\nabla \phi_{rn})^2, \quad (11)$$

$$F_J[\phi_{rn}, \mathbf{A}_r, \mathbf{R}_{n,i}] \rightarrow F_J[\phi_{rn}, \mathbf{R}_{n,i}] = \sum_n \int d^2\mathbf{r} E_J (1 - \cos(\phi_{n+1} - \phi_n)), \quad (12)$$

and use asymptotics  $r_{cut}k_z \gg 1$  in the tilt stiffness (10). Behavior at large distances  $r_\perp \sim \lambda_c$  and  $z \sim a, \lambda$  is important for accurate evaluation of the cutoff in the logarithmically diverging energy of the Josephson vortex. In this range the Josephson term can be linearized and one can use the anisotropic London theory.<sup>11</sup>

### B. Small $c$ axis field: Crossing energy

At small fields and high anisotropy factor pancake vortices do not influence much structure of JVs. However, there is a finite interaction energy between pancake stack and JV (crossing energy) which causes spectacular observable effects, including formation of the mixed chain-lattice state.<sup>6,14,15,16,18</sup> We consider a JV located between the layers 0 and 1 and directed along  $x$  axis with center at  $y = 0$  and a pancake stack located at  $x = 0$  and at distance  $y$  from the JV center. We will calculate structure of the pancake stack and the crossing energy. The JV core structure is defined by the phases  $\phi_n(y)$  obeying the following equation

$$\frac{d^2 \phi_n}{d\tilde{y}^2} + \sin(\phi_{n+1} - \phi_n) - \sin(\phi_n - \phi_{n-1}) = 0 \quad (13)$$

with  $\tilde{y} = y/\lambda_{J0}$ . An accurate numerical solution of this equation has been obtained in Ref. 4. It is described by the approximate interpolation formula<sup>28</sup>

$$\begin{aligned} \phi_n(\tilde{y}) \approx & \arctan \frac{n - 1/2}{\tilde{y}} + \frac{0.35(n - 1/2)\tilde{y}}{((n - 1/2)^2 + \tilde{y}^2 + 0.38)^2} \\ & + \frac{8.81(n - 1/2)\tilde{y}(\tilde{y}^2 - (n - 1/2)^2 + 2.77)}{((n - 1/2)^2 + \tilde{y}^2 + 2.02)^4} \end{aligned} \quad (14)$$

Interaction between the pancake stack and JV appears due to the pancake displacements  $u_n$  under the action of the JV in-plane currents  $j_n(y)$  (see Fig. 1). In the regime of very weak interlayer coupling the energy of the deformed pancake stack is given by

$$E_\times(y) = \int \frac{dk_z}{2\pi} \frac{U_M(k_z)}{2} |u(k_z)|^2 - \sum_n \frac{s\Phi_0}{c} j_n(y) u_n \quad (15)$$

where  $U_M(k_z)$  is the magnetic tilt stiffness of the pancake stack, and  $j_n(y)$  is the reduced superfluid momentum. In this range one can neglect the field contributions in the regular and Josephson energy terms, i.e., drop  $\mathbf{A}_r$ :

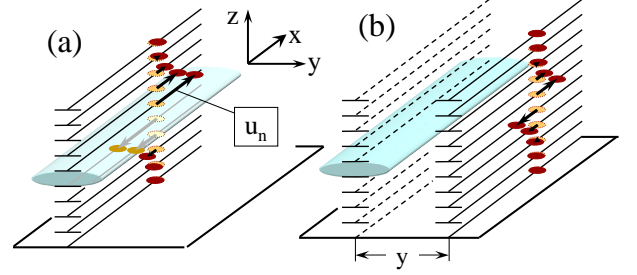


FIG. 1: Configuration of the pancake stack crossing the Josephson vortex: (a) the stack located in the center of JV core and (b) the stack located at a finite distance  $y$  from JV center.

where  $U_M(k_z) = \frac{\Phi_0^2}{2(4\pi)^2\lambda^4} \ln\left(1 + \frac{\lambda^2}{k_z^{-2} + r_w^2}\right)$  is the magnetic tilt stiffness of the pancake stack,

$$j_n(y) \approx \frac{2c\Phi_0}{(4\pi\lambda)^2 \gamma s} p_n\left(\frac{y}{\gamma s}\right)$$

with  $p_n(\tilde{y}) \equiv d\phi_n(\tilde{y})/d\tilde{y}$  being the reduced superfluid momentum, and the JV phase  $\phi_n(\tilde{y})$  is given by approximate formula (14). In particular,  $p_n(0) = -C_n/(n - 1/2)$  with  $C_n \rightarrow 1$  at large  $n$ . Using the precise numerical phases  $\phi_n(\tilde{y})$  we obtain the interpolation formula

$$C_n \approx 1 - 0.265/((n - 0.835)^2 + 0.566),$$

giving  $C_1 \approx 0.55$  and  $C_2 \approx 0.86$ . At large distances from the core,  $n, \tilde{y} \gg 1$ ,  $p_n(\tilde{y})$  is given by

$$p_n(\tilde{y}) = -\frac{n - 1/2}{(n - 1/2)^2 + \tilde{y}^2}.$$

Displacements in the core region have typical wave vectors  $k_z \sim \pi/s$ . In this range one can neglect  $k_z$ -dependence of  $U_M(k_z)$ ,

$$U_M \approx \frac{\Phi_0^2}{(4\pi)^2\lambda^4} \ln \frac{\lambda}{r_w},$$

and rewrite Eq. (15) as

$$E_\times(y) = \sum_n \left( \frac{sU_M}{2} u_n^2 - \frac{s\Phi_0}{c} j_n(y) u_n \right). \quad (16)$$

We neglected weak logarithmic dependence of the tilt stiffness on displacements and the parameter  $r_w$  in  $U_M$  is just a typical value of  $|u_{n+1} - u_n|$ . Minimizing this energy with respect to  $u_n$ , we obtain the pancake displacements

$$u_n(y) = \frac{\Phi_0}{c} \frac{j_n(y)}{U_M} \approx \frac{2\lambda^2}{\gamma s \ln(\lambda/u_n(y))} p_n \left[ \frac{y}{\gamma s} \right]$$

with  $v_n(y) \approx |u_n(y) - u_{n-1}(y)|$  and crossing energy at finite distance  $y$  between the crossing point and the center of JV core

$$E_\times(y) = -\frac{s}{2U_M} \sum_{n=-\infty}^{\infty} \left( \frac{\Phi_0 j_n(y)}{c} \right)^2 \approx -\frac{\Phi_0^2}{4\pi^2 \gamma^2 s \ln(\lambda/u_1(y))} A_\times \left( \frac{y}{\gamma s} \right) \quad (17)$$

with

$$A_\times(\tilde{y}) = \sum_{n=1}^{\infty} [p_n(\tilde{y})]^2 = \sum_{n=-\infty}^{\infty} (1 - \cos(\phi_{n+1} - \phi_n)),$$

where the second identity can be derived from Eq. (13). In particular, for the pancake stack located at the JV center,  $A_\times(0) = 2$  (exact value) and

$$E_\times(0) \approx -\frac{\Phi_0^2}{2\pi^2 \gamma^2 s \ln(3.5\gamma s/\lambda)}. \quad (18)$$

The maximum pancake displacement in the core is given by

$$u_1(0) \approx \frac{2.2\lambda^2}{\gamma s \ln(2\gamma s/\lambda)}. \quad (19)$$

At large distances,  $y \gg \gamma s$ , using asymptotics  $A_\times(\tilde{y}) \approx \pi/4\tilde{y}$ , we obtain

$$E_\times(y) \approx -\frac{\Phi_0^2}{16\pi\gamma y \ln\left(\frac{\beta y^2}{\lambda\gamma s}\right)}, \text{ with } \beta \sim 1. \quad (20)$$

Using numerical calculations, we also obtain the following approximate interpolation formula for the function  $A_\times(\tilde{y})$ , valid for the whole range of  $\tilde{y}$ ,

$$A_\times(\tilde{y}) \approx \frac{\pi/4}{\sqrt{\tilde{y}^2 + y_0^2}} \left( 1 + \frac{a}{\tilde{y}^2 + y_0^2} \right) \quad (21)$$

$y_0 \approx 0.93, a \approx 1.23$

Eqs. (17) and (21) determine the crossing energy at finite distance  $y$  between the crossing point and the center of

the JV core. Below we will use this result to calculate the pinning force which binds the JV to the dilute pancake lattice.

### C. Large $c$ axis field. Approximation of the effective phase stiffness

At high  $c$  axis fields pancakes substantially modify the JV structure. Precise analysis of the JV core in the pancake lattice for the general case requires tedious consideration of many energy contributions (see Section II E below). The situation simplifies considerably in the regime of very high anisotropy  $\gamma \gg \lambda/s$ . In this case one can conveniently describe the JV structure in terms of the effective phase stiffness, which allows us to reduce the problem of a JV in the pancake lattice to the problem of an ordinary JV at  $B_z = 0$ . In Ref. 6 this approach has been used to derive JV structures at high fields  $B_z \gg \Phi_0/4\pi\lambda^2$ . The approach is based on the observation that smooth transverse lattice deformations  $\mathbf{u}_{tn}(\mathbf{r})$  produce large-scale phase variations  $\phi_{vn}(\mathbf{r})$  with  $\nabla\phi_{vn} = 2\pi n_v \mathbf{e}_z \times \mathbf{u}_{tn}$ . This allows us to express the transverse part of the elastic energy,  $F_{v-t}$ , in terms of  $\phi_{vn}(\mathbf{r})$ :

$$F_{v-t} = \int \frac{d\mathbf{k}}{(2\pi)^3} \frac{J_v(B_z, \mathbf{k})}{2s} k_\perp^2 |\phi_v(\mathbf{k})|^2, \quad (22)$$

with the effective phase stiffness  $J_v(B_z, \mathbf{k})$ ,

$$J_v(B_z, \mathbf{k}) = \frac{s(C_{66}k_\perp^2 + U_{44})}{(2\pi n_v)^2} \approx \frac{J}{8\pi n_v \lambda^2} \left( \frac{\lambda^2 k_\perp^2}{2} + \ln \left( 1 + \frac{r_{cut}^2}{k_z^{-2} + r_w^2} \right) \right). \quad (23)$$

Replacing the discrete lattice displacements by the smooth phase distribution is justified at fields  $B_z > \Phi_0/(\gamma s)^2$ . The structure of the JV core is determined by phase deformations with the typical wave vectors  $k_\perp \sim 1/\gamma s < 2/\lambda$  and  $k_z \sim \pi/s > 1/r_w$ . In this range the vortex phase stiffness is  $\mathbf{k}$ -independent, similar to the usual phase stiffness,

$$J_v(B_z) \approx J \frac{B_\lambda}{B_z}, \quad B_\lambda \equiv \frac{\Phi_0}{4\pi\lambda^2} \ln \frac{r_{cut}}{r_w}. \quad (24)$$

The phase stiffness energy (22) has to be supplemented by the Josephson energy. In the core region we can neglect the vector-potentials and write the total energy in terms of  $\phi_{rn}$  and  $\phi_v$  as

$$F = \sum_n \int d^2\mathbf{r} \left( \frac{J}{2} (\nabla\phi_{rn})^2 + \frac{J_v}{2} (\nabla\phi_{vn})^2 + E_J (1 - \cos(\phi_{n+1} - \phi_n)) \right), \quad (25)$$

where, again,  $\phi_n \equiv \phi_{rn} + \phi_{vn}$  is the total phase.

We now investigate the core structure on the basis of the energy (25). Eliminating the regular phase,  $\phi_{rn} = \phi_n - \phi_{vn}$ , and varying the energy with respect to  $\phi_{vn}$  at fixed  $\phi_n$ , we obtain the equation

$$J\Delta\phi_n - (J_v + J)\Delta\phi_{vn} = 0,$$

which gives

$$\phi_{vn} = \frac{J}{J_v + J}\phi_n. \quad (26)$$

Substituting this relation back into the energy (25), we express it in terms of the total phase

$$F = \sum_n \int d^2\mathbf{r} \left( \frac{J_{\text{eff}}}{2} (\nabla\phi_n)^2 + E_J (1 - \cos(\phi_{n+1} - \phi_n)) \right) \quad (27)$$

with the effective phase stiffness  $J_{\text{eff}}$ ,

$$J_{\text{eff}}^{-1} = J^{-1} + J_v^{-1} \text{ or } J_{\text{eff}} = \frac{J}{1 + B_z/B_\lambda}. \quad (28)$$

Note that the smallest stiffness from  $J$  and  $J_v$  dominates in  $J_{\text{eff}}$ .<sup>31</sup> From Eq. (27) we obtain equation for the equilibrium phase

$$J_{\text{eff}} \nabla_y^2 \phi_n + E_J [\sin(\phi_{n+1} - \phi_n) - \sin(\phi_n - \phi_{n-1})] = 0, \quad (29)$$

which has the same form as at zero  $c$  axis field, except that the bare phase stiffness is replaced with the effective phase stiffness  $J_{\text{eff}}$ . For the Josephson vortex located between the layers 0 and 1 the phase satisfies the conditions

$$\phi_1 - \phi_0 \rightarrow \begin{cases} 0, & y \rightarrow \infty \\ 2\pi, & y \rightarrow -\infty \end{cases} \quad (30)$$

Far away from the nonlinear core the phase has the usual form for the vortex in anisotropic superconductor

$$\phi_n(y) \approx \arctan \frac{\lambda_J(n - 1/2)}{y} \quad (31)$$

where the effective Josephson length

$$\lambda_J = \sqrt{J_{\text{eff}}/E_J} = \lambda_{J0}/\sqrt{1 + B_z/B_\lambda}$$

determines the size of the nonlinear core. Therefore, at low temperatures the JV core shrinks in the presence of the  $c$  axis magnetic field due to softening of the in-plane phase deformations. A number of pancake rows within the JV core can be estimated as

$$N_{\text{rows}} \approx \frac{\lambda_{J0}}{\lambda} \sqrt{\frac{\ln(r_{\text{cut}}/r_w)}{4\pi}} \sqrt{\frac{B_z}{B_\lambda + B_z}}. \quad (32)$$

At  $B_z > B_\lambda$  it is almost independent on the field. An approximate solution of Eq. (29) is given by Eq. (14), where the bare Josephson length  $\lambda_{J0}$  has to be replaced by the renormalized length  $\lambda_J$ .

The JV energy per unit length,  $\mathcal{E}_{JV}$ , is given by

$$\mathcal{E}_{JV} = \pi \sqrt{E_J J_{\text{eff}}} \ln \frac{L}{s}, \quad (33)$$

where  $L$  is the cutoff length, which is determined by screening at large distances and will be considered below, in Section IID. From Eqs. (26) and (28) we obtain that the partial contribution of the vortex phase in the total phase,

$$\phi_{vn} = \frac{B_z}{B_z + B_\lambda} \phi_n, \quad (34)$$

continuously grows from 0 at  $B_z \ll B_\lambda$  to 1 at  $B_z \gg B_\lambda$ . From the last equation one can estimate pancake displacements

$$\begin{aligned} u_{x,n}(y) &= \frac{\Phi_0/2\pi}{B_z + B_\lambda} \nabla_y \phi_n \\ &\approx -\frac{\Phi_0/2\pi}{B_z + B_\lambda} \frac{\lambda_J(n - 1/2)}{y^2 + (\lambda_J(n - 1/2))^2}. \end{aligned} \quad (35)$$

The maximum displacement in the core can be estimated as

$$u_{x,0}(0) \approx \frac{2.2\lambda^2}{\lambda_{J0} \ln(r_{\text{cut}}/r_w) \sqrt{1 + B_z/B_\lambda}}. \quad (36)$$

At  $B_z \gg B_\lambda$  this equation can be rewritten in the form

$$\frac{u_{x,0}(0)}{a} \approx \frac{0.58\lambda}{\lambda_{J0} \sqrt{\ln(a/r_w)}}, \quad (37)$$

which shows that condition for applicability of the linear elasticity,  $u_{x,0}(0) \lesssim 0.2a$ , is satisfied if  $\gamma \gtrsim 3\lambda/s$ . Eqs. (31) and (33) describe smooth evolution of the JV structure with increase of concentration of pancakes starting from the usual vortex at  $B_z = 0$ . It is quantitatively valid only at very high anisotropies  $\gamma \gg \lambda/s$  and at low temperatures, when one can neglect fluctuation suppression of the Josephson energy. Thermal motion of the PVs at finite temperatures induces the fluctuating phase  $\tilde{\phi}_{n,n+1}$  and suppresses the effective Josephson energy,  $E_J \rightarrow CE_J$  where  $C \equiv \langle \cos \tilde{\phi}_{n,n+1} \rangle$ . This leads to reduction of the JV energy and thermal expansion of its core.

In the range  $\Phi_0/(\gamma s)^2 < B_z < B_\lambda$  the “crossing energy” regime of Section IIB overlaps with the applicability range of the effective phase stiffness approximation. To check the consistency of these approximations we calculate correction to the JV energy at small fields summing up the crossing energies and compare the result with prediction of the “effective phase stiffness” approximation. The correction to the JV energy is given by

$$\begin{aligned} \delta\mathcal{E}_{JV} &= \frac{1}{a} \sum_{m=-M}^M E_x(mb) \\ &\approx -\frac{\Phi_0 B_z}{8\pi\gamma \ln(\lambda/u_1(0))} \ln \frac{L_y}{\gamma s}, \end{aligned} \quad (38)$$

where  $L_y = Mb$  is the long-range cutoff length. On the other hand, Eqs. (28) and (33) give at  $B_z \ll B_\lambda$

$$\delta\mathcal{E}_{JV} = \pi\sqrt{E_J J} \frac{B_z}{2B_\lambda} \ln \frac{L}{s}. \quad (39)$$

This result is identical to Eq. (38) except for expressions under the logarithms, which are approximate in both cases.

#### D. Large-scale behavior. Screening lengths

In this Section we consider the JV structure at large distances from the core,  $n \gg 1$ ,  $y \gg \lambda_J$ . At large distance screening of supercurrents becomes important and one can not neglect the vector-potential any more. At these scales the phase changes slowly from layer to layer so that one can expand the Josephson energy in Eq. (6) with respect to the phase difference and use the continuous approximation,  $\phi_{n+1} - \phi_n - \frac{2\pi s}{\Phi_0} A_z \rightarrow s \left( \nabla_z \phi - \frac{2\pi}{\Phi_0} A_z \right)$ ,

$$F_J[\phi_n, \mathbf{A}] \rightarrow \tilde{F}_J[\phi, \mathbf{A}] = \int d^3\mathbf{r} \frac{sE_J}{2} \left( \nabla_z \phi - \frac{2\pi}{\Phi_0} A_z \right)^2. \quad (40)$$

This reduces the Lawrence-Doniach model defined by Eqs. (3), (4), (5), and (6) to the anisotropic London

model. Within this model the JV structure outside the core region has been investigated in detail by Savel'ev *et al.*<sup>11</sup>. In this section we reproduce JV structure at large distances using the effective phase stiffness approach. For the vortex energy one still can use Eq. (22) with the full  $k$ -dependent phase stiffness (23). Within these approximations the energy (3) is replaced by

$$F[\phi_r, \phi_v, \mathbf{A}] = F_r[\phi_r, \mathbf{A}_\perp] + F_{v-t}[\phi_v] + \tilde{F}_J[\phi_r + \phi_v, A_z]. \quad (41)$$

Varying the energy with respect to  $\mathbf{A}$ , we obtain

$$\frac{\Phi_0}{2\pi} \nabla_\perp \phi_r - \mathbf{A}_\perp + \lambda^2 \nabla^2 \mathbf{A}_\perp = 0, \quad (42a)$$

$$\frac{\Phi_0}{2\pi} \nabla_z \phi - A_z + \lambda_c^2 \nabla^2 A_z = 0. \quad (42b)$$

It is convenient to perform the analysis of the large-scale behavior in  $\mathbf{k}$ -space. Solving linear equations (42a) and (42b) using Fourier transform,

$$\mathbf{A}_\perp = \frac{\Phi_0}{2\pi} \frac{\nabla_\perp \phi_r}{1 + \lambda^2 k^2}, \quad (43a)$$

$$A_z = \frac{\Phi_0}{2\pi} \frac{\nabla_z \phi}{1 + \lambda_c^2 k^2}, \quad (43b)$$

and excluding  $\mathbf{A}$ , we express the energy in terms of phases

---


$$F = \int \frac{d^3\mathbf{k}}{(2\pi)^3} \left[ \frac{J}{2s} \frac{\lambda^2 k^2}{1 + \lambda^2 k^2} (\nabla_\perp \phi_r)^2 + \frac{J_v(\mathbf{k})}{2s} (\nabla_\perp \phi_v)^2 + \frac{sE_J}{2} \frac{\lambda_c^2 k^2}{1 + \lambda_c^2 k^2} (\nabla_z \phi)^2 \right].$$

Following the procedure of the previous Section, we eliminate  $\phi_r$ , minimize the energy with respect to  $\phi_v$ , and obtain the energy in terms of the total phase

$$F = \int \frac{d^3\mathbf{k}}{(2\pi)^3} \left[ \frac{J_{\text{eff}}(\mathbf{k})}{2s} (\nabla_\perp \phi)^2 + \frac{sE_J(\mathbf{k})}{2} (\nabla_z \phi)^2 \right]. \quad (44)$$

where the effective phase stiffness,  $J_{\text{eff}}(\mathbf{k})$ , and the effective Josephson energy are given by

$$J_{\text{eff}}^{-1}(\mathbf{k}) = J^{-1} \frac{1 + \lambda^2 k^2}{\lambda^2 k^2} + J_v^{-1}(\mathbf{k}) \quad (45a)$$

$$E_J(\mathbf{k}) = E_J \frac{\lambda_c^2 k^2}{1 + \lambda_c^2 k^2} \quad (45b)$$

In the case of the JV, minimization with respect to the phases has to be done with the topological constrain,  $\nabla_z \nabla_y \phi - \nabla_y \nabla_z \phi = 2\pi \delta(y) \delta(z)$ , which gives

$$\nabla_z \phi = \frac{2\pi i k_y J_{\text{eff}}(\mathbf{k})}{J_{\text{eff}}(\mathbf{k}) k_y^2 + s^2 E_J(\mathbf{k}) k_z^2} = \frac{2\pi i k_y (1 + \lambda_c^2 k^2)}{k^2 (1 + \lambda_c^2 k_y^2 + \lambda^2 k_z^2 (1 + w(\mathbf{k})))}, \quad (46a)$$

$$\nabla_y \phi = -\frac{2\pi i k_z s^2 E_J(\mathbf{k})}{J_{\text{eff}}(\mathbf{k}) k_y^2 + s^2 E_J(\mathbf{k}) k_z^2} = -\frac{2\pi i k_z (1 + \lambda^2 k^2)}{k^2 (1 + \lambda_c^2 k_y^2 + \lambda^2 k_z^2 (1 + w(\mathbf{k})))}, \quad (46b)$$

and

$$\begin{aligned}\mathcal{E}_{JV} &= \frac{1}{2} \int d^2\mathbf{k} \frac{sE_J(\mathbf{k})J_{\text{eff}}(\mathbf{k})}{J_{\text{eff}}(\mathbf{k})k_y^2 + s^2E_J(\mathbf{k})k_z^2} \\ &= \frac{J}{2s} \int \frac{d^2\mathbf{k}}{\lambda^{-2} + \gamma^2k_y^2 + k_z^2(1 + w(\mathbf{k}))}\end{aligned}\quad (47)$$

with

$$w(\mathbf{k}) = J/J_v(\mathbf{k}) = \frac{2h}{\lambda^2k_y^2/2 + \ln(1 + k_z^2r_{\text{cut}}^2)} \quad (48)$$

and  $h \equiv 4\pi n_v \lambda^2$ . The integration has to be cut at  $k_z \sim \pi/s$ . In addition, integration with respect to  $k_y$  is typically determined by  $k_y \sim k_z/\gamma$  so that one can neglect in  $w(\mathbf{k})$  the term  $\lambda^2k_y^2/2 \sim \lambda^2k_z^2/2\gamma^2$ , coming from the shear energy, in comparison with the tilt energy term  $\ln(1 + k_z^2r_{\text{cut}}^2)$  and the JV energy reduces to

$$\begin{aligned}\mathcal{E}_{JV} &\approx \frac{J}{2s} \int d^2\mathbf{k} \left( \lambda^{-2} + \gamma^2k_y^2 + k_z^2 + \frac{2hk_z^2}{\ln(1 + k_z^2r_{\text{cut}}^2)} \right)^{-1} \\ &= \frac{\pi J}{\gamma s} \int_0^{k_c} \frac{dk_z}{\sqrt{\lambda^{-2} + k_z^2(1 + 2h/\ln(1 + r_{\text{cut}}^2/(k_z^{-2} + r_w^2)))}}.\end{aligned}\quad (49)$$

A similar formula has been derived in Ref. 11. This formula shows that the small- $k_z$  logarithmic divergence in the integral cuts off at  $k_z = \max(\lambda^{-1}, a^{-1})$ . To reproduce JV energy at  $B_z = 0$  the upper cutoff has to be chosen as  $k_c = 2.36/s$ .

Lets consider in more detail the case of a large  $c$  axis field  $h \gg 1$ , where JV structure is strongly renormalized by the dense pancake lattice. Formula for the JV energy simplifies in this limit to

$$\mathcal{E}_{JV} \approx \frac{\pi J}{\gamma s \sqrt{2h}} \int_0^{k_c} \sqrt{\ln(1 + 0.05a^2/(k_z^{-2} + r_w^2))} \frac{dk_z}{k_z}.$$

To estimate this integral, we split the integration region into two intervals,  $1/r_w \lesssim k_z \lesssim \pi/s$  and  $\pi/a \lesssim k_z \lesssim 1/r_w$ , and obtain

$$\mathcal{E}_{JV} \approx \frac{\pi J}{\gamma s \sqrt{h}} \left( \sqrt{\ln\left(\frac{0.2a}{r_w}\right)} \ln \frac{2.4r_w}{s} + \frac{2}{3} \left[ \ln\left(\frac{0.2a}{r_w}\right) \right]^{3/2} \right).$$

Note that the long-range contribution to the energy scales as a logarithm to the power 3/2.

### 1. Magnetic field of Josephson vortex

Using Eqs. (46) and (43) we obtain for the JV magnetic field (see also Ref. 11)

$$B_x(\mathbf{k}) = \frac{\Phi_0}{1 + \lambda_c^2k_y^2 + \lambda^2k_z^2(1 + w(\mathbf{k}))}, \quad (50)$$

where  $w(\mathbf{k})$  is given by Eq. (48). Let us consider the case of large magnetic fields  $B > B_\lambda$ . In a wide region,  $\lambda < \sqrt{y^2 + (\gamma z)^2} < \lambda_c$ , the magnetic field in real space is approximately given by

$$\begin{aligned}B_x(y, z) &\approx \Phi_0 \int \frac{dk_y dk_z}{4\pi^2} \exp(ik_y y + ik_z z) \left( \lambda_c^2k_y^2 + \frac{2\lambda^2 h k_z^2}{\ln(1 + a^2k_z^2/20)} \right)^{-1} \\ &= \frac{\Phi_0}{2\pi\lambda\lambda_c\sqrt{2h}} \int_0^\infty dk_z \frac{\sqrt{\ln(1 + a^2k_z^2/20)}}{k_z} \exp\left(-\frac{\sqrt{2h}k_z|y|}{\gamma\sqrt{\ln(1 + a^2k_z^2/20)}}\right) \cos(k_z z)\end{aligned}\quad (51)$$

One can estimate from this expression the JV maximum field as

$$B_x(0, 0) \approx \frac{\Phi_0}{3\pi\lambda\lambda_c\sqrt{h}} \left( \ln \frac{a}{z_c} \right)^{3/2} \quad (52)$$

and this field decays at the scale  $\sim a/4.5$  in the  $z$  direction and at the scale  $\gamma a^2/20\lambda$  in the  $y$  direction. The



magnetic flux concentrated at this region is estimated as  $\Phi \approx \Phi_0/(1 + 2.8h^2)$ . The residual flux,  $\Phi_0 - \Phi$ , is distributed over the pancake lattice at much larger distances.

Due to the elasticity of the pancake lattice, the behavior at large distances is very unusual. The limiting expression for  $B_x(\mathbf{k})$  at  $\mathbf{k} \rightarrow 0$  is given by

$$B_x(\mathbf{k}) \approx \Phi_0 \left( 1 + \frac{hk_z^2}{k_y^2/4 + k_z^2/(2.8h)} \right)^{-1} \quad (53)$$

Formally, the total flux of JV is given by the limit

$$\Phi = \lim_{\mathbf{k} \rightarrow 0} B_x(\mathbf{k})$$

However this limit depends on the order of limits  $\lim_{k_y \rightarrow 0}$  and  $\lim_{k_z \rightarrow 0}$

$$\begin{aligned} \lim_{k_z \rightarrow 0} \lim_{k_y \rightarrow 0} B_x(\mathbf{k}) &= \frac{\Phi_0}{1 + 2.8h^2} \approx \frac{\Phi_0}{2.8h^2} \\ \lim_{k_y \rightarrow 0} \lim_{k_z \rightarrow 0} B_x(\mathbf{k}) &= \Phi_0 \end{aligned}$$

This apparent paradox can be resolved by calculating the field distribution in the real space

$$\begin{aligned} B_x(y, z) &\approx \frac{1}{2} \left( 1 + \frac{1}{2.8h^2} \right) \Phi_0 \delta(\mathbf{r}) \\ &- \left( 1 - \frac{1}{2.8h^2} \right) \frac{\Phi_0}{\pi\sqrt{h}} \frac{4y^2 - z^2/h}{(4y^2 + z^2/h)^2}, \end{aligned} \quad (54)$$

This expression clearly shows that the screening is incomplete: the field at large scales has a slowly decaying  $1/r^2$  tail. The magnetic flux through the large size box  $L_y \times L_z$  is given by

$$\Phi(L_y, L_z) = \Phi_0 \left( 1 - \left( 1 - \frac{1}{2.8h^2} \right) \frac{2}{\pi} \arctan \left( \frac{2\sqrt{h}L_y}{L_z} \right) \right)$$

and the limiting value of the total flux at  $L_y, L_z \rightarrow \infty$  depends on the aspect ratio  $L_y/L_z$ .

### E. Quantitative analysis of the core structure

The simple “effective phase stiffness” approximation, described in Section II C, is only valid if  $\gamma$  is significantly larger than  $\lambda/s$ . In BSCCO, even at low temperatures,  $\gamma$  is at most 3 – 4 times larger than  $\lambda/s$ . Moreover, it always approaches  $\lambda/s$  at  $T \rightarrow T_c$ . In this section we extend our analysis to the region  $\gamma \sim \lambda/s$ . We consider JV structure at low temperatures and not very small  $c$  axis field,  $B_z > \Phi_0/(\gamma s)^2$ . The structure of JV core is completely determined by the displacements of pancake vortices and phase distribution. The equilibrium pancake displacements depend only on the layer index and on coordinate, perpendicular to the direction of the vortex (see Fig. 2). Therefore, the energy can be expressed in terms

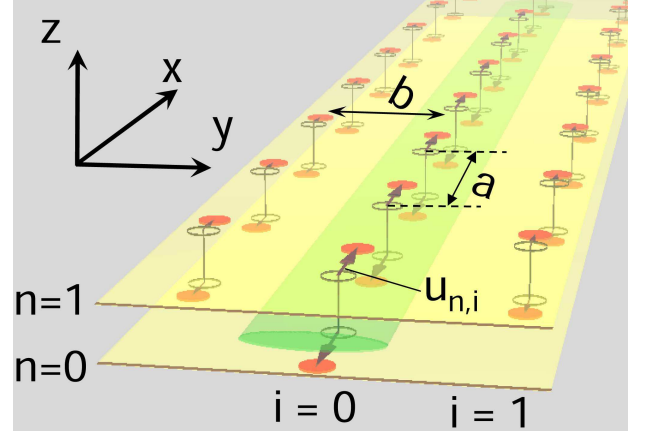


FIG. 2: Displacements of the pancake rows in the JV core.

of the displacements of the vortex rows  $u_{n,i}$ . Different representations for the magnetic interaction between the vortex rows  $U_{Mr}(u_{n,i} - u_{m,j}, n - m)$  are considered in Appendix A. We will operate with the phase perturbation  $\phi_n(\mathbf{r})$  with respect to equilibrium phase distribution of the perfectly aligned pancake crystal. We split this phase into the contribution, averaged over the JV direction ( $x$  axis),  $\bar{\phi}_n(y)$ , and the oscillating in the  $x$  direction contribution,  $\tilde{\phi}_n(x, y)$ . Pancake displacements induce jumps of the average phase at the coordinates of the vortex rows  $Y_i$ ,  $\bar{\phi}_n(Y_i + 0) - \bar{\phi}_n(Y_i - 0) = 2\pi u_{n,i}/a$ . The oscillating phase induced by the row displacements becomes negligible already at the neighboring row. This allows us to separate the local contribution to the Josephson energy coming from  $\tilde{\phi}_n(x, y)$  (see Appendix B) and reduce initially three-dimensional problem to the two-dimensional problem of finding the average phase and row displacements. Further on we operate only with the averaged phase and skip the accent “-” in the notation  $\bar{\phi}_n(y)$ . We again split the total phase into the continuous regular phase,  $\phi_{rn}(y)$ , and the vortex phase,  $\phi_{vn}(y)$ ,  $\phi_n(y) = \phi_{rn}(y) + \phi_{vn}(y; u_{n,i})$ . The vortex phase is composed of jumps at the row positions  $Y_i$ ,

$$\phi_{vn}(y; u_{n,i}) = -\frac{2\pi}{a} \sum_i u_{n,i} \Theta(Y_i - y), \quad (55)$$

where  $\Theta(y)$  is the step-function ( $\Theta(y) = 1$  ( $0$ ) at  $y > 0$  ( $y < 0$ )). In the effective phase stiffness approach of Section II C we used a coarse-grained continuous approximation for this phase. We neglect  $x$ -dependent contribution in the regular phase, which is small at  $B > \Phi_0/(\gamma s)^2$ . Collecting relevant energy contributions, we now write the energy per unit length in terms of the regular phase,

$\phi_{rn}(y)$ , and the row displacements,  $u_{n,i}$ ,

$$\begin{aligned} \mathcal{E}_J = & \sum_n \int dy \left[ \frac{J}{2} \left( \frac{d\phi_{rn}}{dy} \right)^2 + E_J (1 - \cos(\phi_{n+1} - \phi_n)) \right] \\ & + \frac{1}{2} \sum_{n,m,i,j} \tilde{U}_{Mr}(u_{n,i} - u_{m,j}, Y_{i,j}, n - m) \\ & + \sum_{n,i} \mathcal{E}_{Josc}(u_{n+1,i} - u_{n,i}, \phi_{n+1,i} - \phi_{n,i}) \end{aligned} \quad (56)$$

where

- $\phi_n(y) \equiv \phi_{rn}(y) + \phi_{vn}(y; u_{n,i})$  is the total phase;
- $U_{Mr}(x_{n,i} - x_{m,j}, Y_{i,j}, n - m)$  is the magnetic interaction between the vortex rows separated by distance  $Y_{i,j} = Y_i - Y_j = b(i - j)$  (see Appendix A),

$$\begin{aligned} \tilde{U}_{Mr}(u_{n,i} - u_{m,j}, \dots) \equiv & U_{Mr}(X_{i-j} + u_{n,i} - u_{m,j}, \dots) \\ & - U_{Mr}(X_{i-j}, \dots). \end{aligned}$$

is the variation of this interaction caused by pancake row displacements,  $X_i = 0$  for even  $i$  and  $X_i = a/2$  for odd  $i$ .

$\tilde{U}_{Mr}(x, y, n)$  is periodic with respect to  $x$ ,

$$\tilde{U}_{Mr}(x + a, y, n) = \tilde{U}_{Mr}(x, y, n);$$

- $\mathcal{E}_{Josc}(u_{n+1,i} - u_{n,i}, \phi_{n+1,i} - \phi_{n,i})$  is the local Josephson energy due to the oscillating component of the phase difference (see Appendix B) with

$$\phi_{n,i} \equiv \phi_{rn}(Y_i) + \pi \frac{u_{n,i}}{a} - \frac{2\pi}{a} \sum_{j>i} u_{n,j} \Theta(Y_j - y)$$

being the external phase at  $i$ -th rows and  $n$ -th layer.

The energy (56) describes JV structure at distances  $r_\perp \ll \lambda_c$  and  $z \ll a, \lambda$  from its center.

To facilitate calculations we introduce the reduced coordinates

$$\tilde{y} = \frac{y}{\gamma s}, \quad v_{ni} = \frac{u_{ni}}{a},$$

and represent the energies in the scaling form. Magnetic interaction between the rows we represent as

$$U_{Mr}(x, y, n) = \frac{\pi J a}{\lambda^2} \mathcal{V}_{Mr}\left(\frac{x}{a}, \frac{y}{a}, n\right),$$

---

where

$$\begin{aligned} \mathcal{V}_{Mr}(x, y, n) = & -\frac{\lambda^2}{a^2} \left( \delta_n - \frac{s}{2\lambda} \exp\left(-\frac{s|n|}{\lambda}\right) \right) \ln[1 - 2 \cos 2\pi x \exp(-2\pi|y|) + \exp(-4\pi|y|)] \\ & + \frac{s\lambda}{2a^2} \sum_{m=-\infty}^{\infty} u\left(\frac{\sqrt{y^2 + (x-m)^2}}{\lambda/a}, \frac{s|n|}{\lambda}\right) \end{aligned}$$

and  $u(r, z)$  is defined by Eq. (8). Note that at  $x, y \rightarrow 0$   $\mathcal{V}_{Mr}(x, y, n)$  remains finite for  $n \neq 0$  because, logarithmic divergency in the first term is compensated by logarithmic divergency of the  $m = 0$  term in the sum. At  $\rho^2 \equiv x^2 + y^2 \rightarrow 0$ , using asymptotics  $u(\rho, z) \approx \exp(-z) \left( -\gamma_E - \ln\left(\frac{\rho^2}{2z}\right) \right) + \exp(z) E_1(2z)$  with  $\gamma_E = 0.5772$ , we obtain the limiting value of  $\mathcal{V}_{Mr}(x, y, n)$  at  $n \neq 0$

$$\mathcal{V}_{Mr}(0, 0, n) = \frac{s\lambda}{2a^2} \left[ \exp\left(-\frac{s|n|}{\lambda}\right) \left( \ln\left[\frac{8\pi^2 s|n|\lambda}{a^2}\right] - \gamma_E \right) + \exp\left(\frac{s|n|}{\lambda}\right) E_1\left(\frac{2s|n|}{\lambda}\right) + 2 \sum_{m=1}^{\infty} u\left(\frac{am}{\lambda}, \frac{s|n|}{\lambda}\right) \right].$$

The local Josephson energy can be represented as

$$\mathcal{E}_{Josc}(u, \phi) = 2E_J a \cos(\phi) \mathcal{J}(u/a),$$

where  $\mathcal{J}(v)$  is dimensionless function,  $\mathcal{J}(v) \approx \frac{\pi}{4} v^2 \ln \frac{0.39}{v}$  at  $v \ll 1$  (see Appendix B). In reduced units the total energy takes the form

$$\begin{aligned} \mathcal{E}_J / \varepsilon_{J0} = & \sum_n \int d\tilde{y} \left[ \frac{1}{2} \left( \frac{d\phi_{rn}}{d\tilde{y}} \right)^2 + 1 - \cos(\phi_{n+1} - \phi_n) \right] \\ & + \frac{\pi \gamma s a}{2\lambda^2} \sum_{n,m,i,j} \tilde{\mathcal{V}}_{Mr}(v_{n,i} - v_{m,j}, \frac{\tilde{Y}_{i,j}}{a_\gamma}, n - m) \\ & + \frac{2a}{\gamma s} \sum_{n,i} \mathcal{J}(v_{n+1,i} - v_{n,i}) \cos(\phi_{n+1,i} - \phi_{n,i}) \end{aligned} \quad (57)$$

where  $\varepsilon_{J0} \equiv E_J \gamma s \equiv J/\gamma s$  is the JV energy scale,  $\phi_n(y) = \phi_{rn}(y) - 2\pi \sum_i v_{n,i} \Theta(Y_i - y)$  and  $a_\gamma \equiv a/\gamma s$ . Varying the energy, we obtain equations for  $v_{n,i}$  and  $\phi_n$

$$\nabla_y \phi_{rn}(Y_i) + \frac{\gamma s a}{2\lambda^2} \sum_{m,j} \mathcal{F}_{Mr}(v_{n,i} - v_{m,j}, \frac{\tilde{Y}_{i,j}}{a_\gamma}, n - m) + \frac{a}{\pi \gamma s} \sum_{\delta=\pm 1} \cos(\phi_{n,i} - \phi_{n+\delta,i}) \mathcal{F}_J(v_{n,i} - v_{n+\delta,i}) = 0, \quad (58a)$$

$$\frac{d^2 \phi_{rn}}{d\tilde{y}^2} + \sin(\phi_{n+1} - \phi_n) - \sin(\phi_n - \phi_{n-1}) = 0. \quad (58b)$$

Here  $\mathcal{F}_{Mr}(x, y, n) \equiv -\nabla_x \mathcal{V}_{Mr}(x, y, n)$  is the magnetic interaction force between the vortex rows

$$\mathcal{F}_{Mr}(x, y, n) = \frac{2\pi\lambda^2}{a^2} \left( \delta_n - \frac{s}{2\lambda} \exp\left(-\frac{s|n|}{\lambda}\right) \right) \frac{\sin 2\pi x}{\cosh 2\pi|y| - \cos 2\pi x} + \frac{s\lambda}{a^2} \sum_m \frac{x - m}{(x - m)^2 + y^2} \exp\left(-\frac{\sqrt{(x - m)^2 + y^2 + z^2}}{\lambda/a}\right).$$

and  $\mathcal{F}_J(v, \phi) = -\partial \mathcal{J}(v)/\partial v \approx -(\pi/2)v \ln(0.235/v)$  at  $v \ll 1$ . The derivative of the regular phase has jumps at the positions of the rows

$$\frac{d\phi_{rn}}{d\tilde{y}}(\tilde{Y}_i + 0) - \frac{d\phi_{rn}}{d\tilde{y}}(\tilde{Y}_i - 0) = \frac{2a}{\gamma s} \sum_{\delta=\pm 1} \mathcal{J}(v_{n+\delta,i} - v_{n,i}) \sin(\phi_{n+\delta,i} - \phi_{n,i}). \quad (59)$$

To find JV structure at low temperatures one has to solve Eqs. (58a), (58b), and (59) with condition (30).

Let us consider in more detail magnetic interactions between vortex rows, i.e., the term with  $\mathcal{F}_{Mr}$  in Eq. (58a). Firstly, one can observe that the dominating contributions to the sum over the layer index  $m$  and row index  $j$  come from rows in the same layer,  $m = n$ , and rows in the same of stacks,  $j = i$ . The former sum determines the shear stiffness, while the latter one determines the magnetic tilt stiffness.

$$\sum_{m,j} \mathcal{F}_{Mr}(v_{n,i} - v_{m,j}, \frac{\tilde{Y}_{i,j}}{a_\gamma}, n - m) \approx f_{\text{shear}}[v_{n,i}] + f_{\text{tilt}}[v_{n,i}] \quad (60)$$

with

$$f_{\text{shear}}[v_{n,i}] = \sum_{j \neq i} \mathcal{F}_{Mr}(v_{n,i} - v_{n,j}, \frac{\tilde{Y}_{i,j}}{a_\gamma}, 0) \quad (61)$$

$$f_{\text{tilt}}[v_{n,i}] = \sum_{m \neq n} \mathcal{F}_{Mr}(v_{n,i} - v_{m,i}, 0, n - m) \quad (62)$$

The sum over the rows in  $f_{\text{shear}}[v_{n,i}]$  converges very fast and effectively is determined by the first two neighboring rows. Note that skipping the terms with  $m \neq n$  in  $f_{\text{shear}}[v_{n,i}]$  is completely justified in the limit  $a < \lambda$  but leads to overestimation of the shear energy in the limit  $a > \lambda$ . However in this limit the shear energy has al-

ready a very weak influence on JV properties. The sum over the layers in  $f_{\text{tilt}}[v_{n,i}]$  is determined by large number of the layers of the order of  $a/s$  or  $\lambda/s$ . If we consider layer  $n$  close to the JV core, then the interaction force with row in the layer  $m$ , in the same stack with  $n \ll m \ll a/s, \lambda/s$  is given by  $\mathcal{F}_{Mr}(v_{n,i} - v_{m,i}, 0, n - m) \approx -(v_{n,i} - v_{m,i})/2(m - n)$ . Interactions with remote layers give large contributions even if displacements in these layers are small,  $v_{m,i} \ll v_{n,i}$ . A useful trick to treat this situation is to separate interaction of a given pancake row with the *aligned* stack pancake rows:

$$f_{\text{tilt}}[v_{n,i}] = \sum_{m \neq n} \tilde{\mathcal{F}}_{Mr}(v_{n,i} - v_{m,i}, 0, n - m) + f_{\text{cage}}(v_{n,i})$$

with

$$\tilde{\mathcal{F}}_{Mr}(v_{n,i} - v_{m,i}, 0, n - m) = \mathcal{F}_{Mr}(v_{n,i} - v_{m,i}, 0, n - m) - \mathcal{F}_{Mr}(v_{n,i}, 0, n - m)$$

and

$$f_{\text{cage}}(v) = \sum_{m \neq 0} \mathcal{F}_{Mr}(v, 0, m)$$

is the interaction force of a chosen pancake row with the aligned stack of rows (“cage” force), for which we derive a useful representation

$$f_{\text{cage}}(v) = -\sum_{l=1}^{\infty} \frac{4\pi \sin(2\pi l v)}{\sqrt{(a/\lambda)^2 + (2\pi l)^2} \left( \sqrt{(a/\lambda)^2 + (2\pi l)^2} + 2\pi l \right)}.$$

At  $v \ll 1 \ll \lambda/a$  this equation gives  $f_{\text{cage}}(v) \approx -v \ln(0.433/v)$ .  $\tilde{\mathcal{F}}_{Mr}(v_{n,i} - v_{m,i}, 0, n - m)$  behaves as  $v_{m,i}/2(m - n)$  at large  $m$  and decays with increase of  $m$  much faster than  $\mathcal{F}_{Mr}(v_{n,i} - v_{m,i}, 0, n - m)$ . The same splitting can be made in the magnetic coupling energy:

$$\begin{aligned} \frac{1}{2} \sum_{m \neq n} \mathcal{V}_{Mr}(v_n - v_m, n - m) &= \sum_{|m| > |n|} (\mathcal{V}_{Mr}(v_n - v_m, n - m) - \mathcal{V}_{Mr}(v_n, n - m) - \mathcal{V}_{Mr}(v_m, n - m)) \\ &+ \sum_n v_{\text{cage}}(v_n) \end{aligned}$$

with

$$\begin{aligned} v_{\text{cage}}(v) &= \sum_{n \neq 0} \mathcal{V}_{Mr}(v, n) \\ &= \sum_{l=1}^{\infty} \frac{2(1 - \cos(2\pi lv))}{l \sqrt{(a/\lambda)^2 + (2\pi l)^2} \left( \sqrt{(a/\lambda)^2 + (2\pi l)^2} + 2\pi l \right)} \end{aligned}$$

This function has simple asymptotics at  $v \ll 1 \ll \lambda/a$ ,  $v_{\text{cage}}(v) \approx (v^2/2) \ln(0.713/v)$ .

We demonstrate now that in the limit  $\gamma \gg \lambda/s$  Eqs. (58a) and (58b) reproduce the JV structure obtained within the effective phase stiffness approximation. One can show that in this limit the local Josephson energy influences weakly the JV structure. We calculate correction to the JV energy due to this term in the Appendix C. The dominating contribution to the magnetic interaction between the pancake rows,  $\sum_{m,j} \mathcal{F}_{Mr}(v_{n,i} - v_{m,j}, \frac{Y_{i,j}}{a_\gamma}, n - m)$ , comes from the tilt force (62), which with good accuracy can be described by the cage force  $f_{\text{cage}}(v_{n,i})$  in the limit of small  $v_{n,i}$ ,  $f_{\text{cage}}(v) \approx -v \ln(C/v)$  with  $C \approx 0.433$ . Further estimate shows, that the term  $\sum_{m \neq n} \tilde{\mathcal{F}}_{Mr}(v_{n,i} - v_{m,i}, 0, n - m)$  in Eq. (62) amounts to the replacement of numerical constant  $C$  under the logarithm by slowly changing function of the order of unity. Because of slow space variations, the discrete row displacements  $v_{n,i}$  can be replaced by the continuous displacement field  $v_n(y)$ . Within these approximations Eq. (58a) reduces to

$$\nabla_y \phi_{rn} \approx \frac{\gamma s a}{2\lambda^2} v_n(y) \ln \frac{C}{v_n(y)}$$

Replacing  $v(y)$  by the vortex phase  $\phi_{vn}(y)$  obtained by coarse-graining of Eq. (55),  $v_n(y) = (b/2\pi\gamma s) \nabla_y \phi_{vn}(y)$ , we obtain

$$\nabla_y \phi_{rn} \approx \frac{B_\lambda}{B_z} \nabla_y \phi_{vn}$$

Note that we replaced  $v_n(y)$  in  $\ln[C/v_n(y)]$  by its typical value and absorbed the logarithmic factor into the definition of  $B_\lambda$  (24). From the last equation we obtain  $\phi_{rn} = (B_\lambda/B_z) \phi_{vn}$  and

$$\phi_n = \left(1 + \frac{B_z}{B_\lambda}\right) \phi_{rn}$$

Therefore Eq. (58b) reduces to

$$-\frac{1}{1 + \frac{B_z}{B_\lambda}} \frac{d^2 \phi_n}{dy^2} + \sin(\phi_n - \phi_{n+1}) + \sin(\phi_n - \phi_{n-1}) = 0,$$

which is just dimensionless version of Eq. (29).

#### 1. Numerical calculations of JV core structure. Crossover to solitonlike cores.

To explore the JV core structure, we solved Eqs. (58a) and (58b) numerically for different ratios  $\lambda/\gamma s$  and different magnetic fields. We used a relaxation technique to find the equilibrium displacements of the pancake rows and the continuous regular phase. Typically, we solved equations for 20 layers and the in-plane region  $0 < \tilde{y} < 20$ .

To test the “effective phase stiffness” model and to calculate uncertain numerical factors, we start from the case of large anisotropies,  $\gamma \gg \lambda/s$ . Figure 3 shows the grey level plots of the cosine of the phase difference between two central layers of JV,  $\cos \Theta$ ,  $\Theta \equiv \phi_1 - \phi_0 \equiv 2\phi_1$ , for  $\lambda = 0.2\gamma s$ . Fig. 4 shows  $y$  dependence of the total phase difference  $\Theta$  and the contribution to this phase coming from the regular phase for the same parameters. As one can see, at  $B \gtrsim \Phi_0/(\gamma s)^2$  the core region covers several pancake rows. At high fields the core size shrinks so that the number of rows in the core does not change, in agreement with the “effective phase stiffness” model. From Fig. 4 one can see that the fraction of the regular phase in the total phase progressively decreases with increase of magnetic field. For the field  $8\Phi_0/(\gamma s)^2$  we also plotted  $\Theta(y)$  dependence from the “effective phase stiffness” model, assuming  $B_\lambda = 2.1\Phi_0/4\pi\lambda^2$ . One can see that the numerically calculated dependence is reasonably well described by this model.

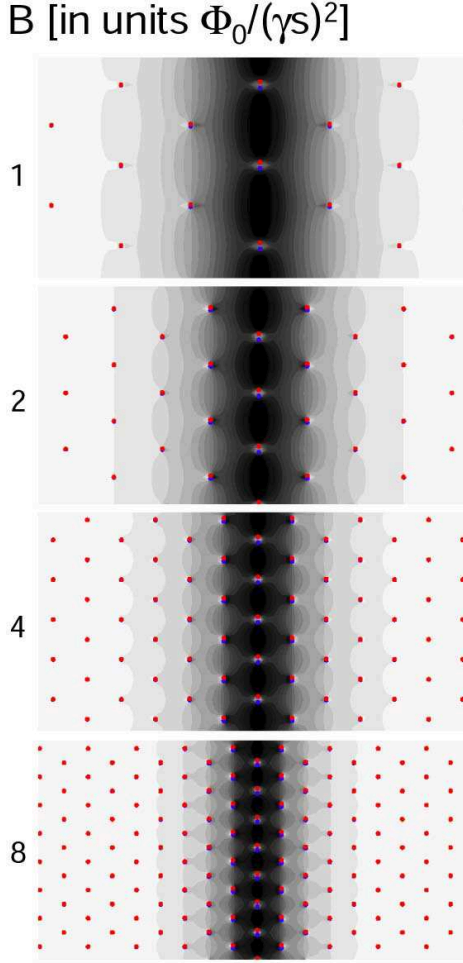


FIG. 3: Grey level plots of cosine of the phase difference between two central layers of JV,  $\cos \Theta$ , for  $\lambda = 0.2\gamma s$  and several magnetic fields (dark regions correspond to  $\cos \Theta \sim -1$  and white regions correspond to  $\cos \Theta \sim 1$ ). The total size of displayed region in the horizontal direction is  $6\gamma s$ . One can see that in this regime several pancake rows fit inside the core region. At high fields the size of the core shrinks so that the number of pancake rows inside the core remains constant.

We now extend study of the core structure to moderate anisotropies  $\sim \lambda/s$ . At Fig. 5 we plot the maximum pancake displacement  $u_{\max}$  in the core region normalized to the lattice constant  $a$  as function of magnetic field for different  $\lambda/\gamma s$ . The maximum displacement approximately saturates at a finite fraction of lattice constant at high field (at high  $\lambda/\gamma s$  one can actually observe a slight decrease of  $u_{\max}/a$  with field). Fig. 6 shows dependence of  $u_{\max}/a$  on  $\lambda/\gamma s$  for fixed field  $B = 10\Phi_0/(\gamma s)^2$ . Dashed line shows prediction of the “effective phase stiffness” model given by Eq. (37). One can see that this equation correctly predicts maximum displacement for  $\lambda/\gamma s < 0.35$ . Important qualitative change occurs at  $\lambda/\gamma s > 0.35$ , where the maximum displacement  $u_{\max}(0)$  exceeds  $a/4$ . This means that the pancakes initially be-

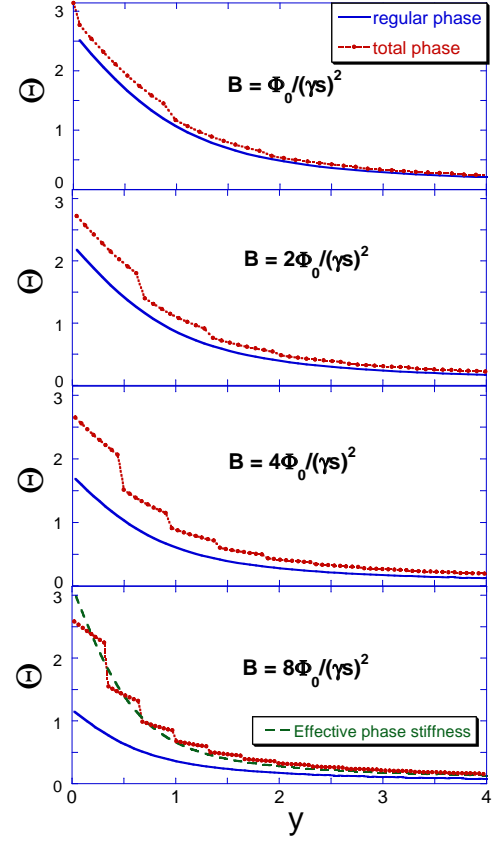


FIG. 4: Coordinates dependence of the phase difference between two central layers,  $\Theta = \phi_1 - \phi_0$ , for  $\lambda/\gamma s = 0.2$  and different magnetic fields. Circles connected by dotted lines represent total phase difference, solid lines show contributions from the regular phase. Jumps of the total phase difference at the positions of pancake rows are caused by pancake displacement and represent the vortex phases. In the lower plot dashed line represents prediction of the “effective phase stiffness” model with  $B_\lambda = 2.1\Phi_0/4\pi\lambda^2$ .

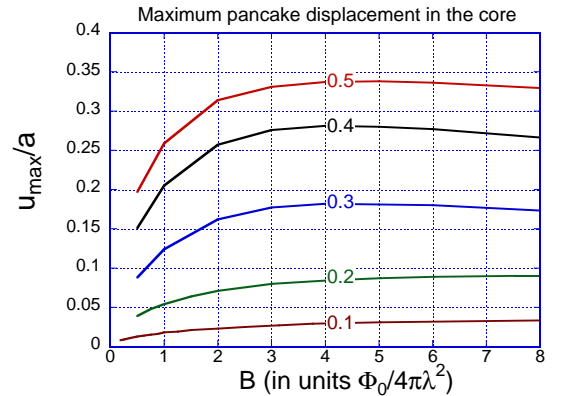


FIG. 5: Field dependencies of the maximum pancake displacement in the core at different ratios  $\lambda/\gamma s$  (the curves are labelled by this ratio).

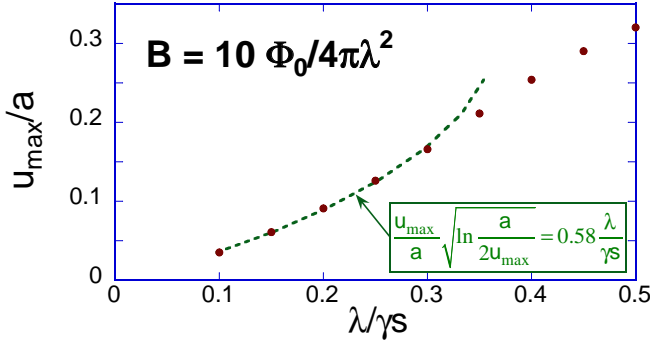


FIG. 6: Dependence of the maximum pancake displacement in the core on the ratio  $\lambda/\gamma s$  at  $B = 10\Phi_0/4\pi\lambda^2$ . Dashed line represents prediction of the “effective phase stiffness” model (37).

longing to the neighboring stacks become closer than the pancakes belonging to the same stack. This can be viewed as switching of the vortex lines in the central layer of JV. This switching is clearly observed in Fig. 7, which shows pancake displacements in the central row of pancake stacks and its neighboring row for two values of the ratio  $\lambda/\gamma s$ , 0.3 and 0.5, and several fields. For  $\lambda/\gamma s = 0.5$  configuration of the pancake rows in the central stack is very similar to the classical soliton (“kink”) of the stationary sine-Gordon equation: the stacks smoothly transfer between the two ideal lattice position in the region of the core. Simplified approximate description of such solitonlike structure in the case  $\gamma s < \lambda$  is presented below in Sec. II F. Fig. 8 shows distribution of cosine of inter-layer phase difference between two central layers,  $\cos\Theta$ . As one can see, at  $\lambda/\gamma s = 0.3$  there are still extended regions of large phase mismatch in the JV core (dark regions), while for  $\lambda/\gamma s = 0.5$  these regions are almost eliminated by large pancake displacements in the core.

#### F. Simple model for solitonlike cores at moderate anisotropies

In this Section we consider the structure of the JV core for moderate anisotropies  $\gamma s < 0.5\lambda$  and high fields  $B > \Phi_0/4\pi\lambda^2$ . Estimate (37) and numerical calculations show that at sufficiently small anisotropy,  $\gamma < 0.5\lambda/s$ , the maximum displacement in the core region exceeds a quarter of the lattice spacing. This means that distance between displaced pancakes belonging to the same vortex line,  $2u_{x,0}(0)$ , becomes larger than the distance between pancakes initially belonging to the neighboring lines,  $a - 2u_{x,0}(0)$ . This can be viewed as switching of the vortex lines in the central layer of JV. At lower anisotropies pancake stacks in the central row acquire structure, similar to the soliton of the stationary sine-Gordon model: in the core region they displace smoothly between the two ideal lattice position (see Fig. 7 for  $\lambda/\gamma s = 0.5$ ). In such

configuration a strong phase mismatch between the two central layers is eliminated, which saves the Josephson energy in the core region. On the other hand, large pancake displacements lead to greater loss of the magnetic coupling energy. To describe this soliton structure, we consider a simplified model, in which we (i) keep only displacements in the central row  $v_{n,0} \equiv v_n$ , (ii) use the cage approximation for magnetic interactions and (iii) neglect the shear energy. All these approximations are valid close to the JV center. At  $n > 0$  we redefine displacements as  $v_n \rightarrow 1 + v_n$ . The redefined displacements depend smoothly on the layer index,  $v_{n+1} - v_n \ll 1$ , so that one can replace the layer index  $n$  by continuous variable  $z = ns$ ,  $u_n \rightarrow u(z)$ , and use elastic approximation for the Josephson tilt energy:

$$\mathcal{E}_{\text{core}} \approx \int dz \left( \frac{\pi E_J s \mathcal{L}_J}{2a} \left( \frac{du}{dz} \right)^2 + \frac{\pi J a}{s \lambda^2} v_{\text{cage}} \left( \frac{u}{a} \right) \right), \quad (63)$$

where the logarithmic factor  $\mathcal{L}_J$  is estimated as  $\mathcal{L}_J \approx \ln \left[ 0.39(a/s) |du/dz|^{-1} \right]$  and

$$v_{\text{cage}}(v) \approx \sum_{l=1}^{\infty} \frac{1 - \cos(2\pi l v)}{(2\pi)^2 l^3}$$

is the magnetic cage. For estimates, we replace  $\mathcal{L}_J$  by a constant substituting a typical value for  $du/dz$  under the logarithm. The equilibrium reduced displacement  $v = u/a$  is determined by equation

$$-\frac{d^2 v}{dz^2} + \frac{\gamma^2}{\mathcal{L}_J \lambda^2} v'_{\text{cage}}(v) = 0. \quad (64)$$

Its solution is implicitly determined by the integral relation

$$\int_{1/2}^v \frac{dv}{\sqrt{v_{\text{cage}}(v)}} = \frac{A \gamma z}{\lambda}$$

with  $A = \sqrt{\frac{2}{\mathcal{L}_J}}$ . Therefore a typical size of the soliton is given by

$$z_s \approx \lambda/\gamma$$

and the applicability condition of this approach  $z_s \gg s$  is equivalent to  $\gamma s \ll \lambda$ . In fact, an accurate numerical calculations of the previous section show that the core acquires the solitonlike structure already at  $\gamma s \lesssim 2\lambda$ . The core energy is given by

$$\mathcal{E}_{\text{core}} \approx \frac{a \pi \sqrt{2 J E_J \mathcal{L}_J}}{\lambda} \int_0^1 dv \sqrt{v_{\text{cage}}(v)}$$

At  $a \ll \lambda$  numerical evaluation of the integral gives  $\int_0^1 dv \sqrt{v_{\text{cage}}(v)} \approx 1.018/2\pi$  and we obtain

$$\mathcal{E}_{\text{core}} \approx \sqrt{J E_J \frac{\mathcal{L}_J a}{2 \lambda}}.$$



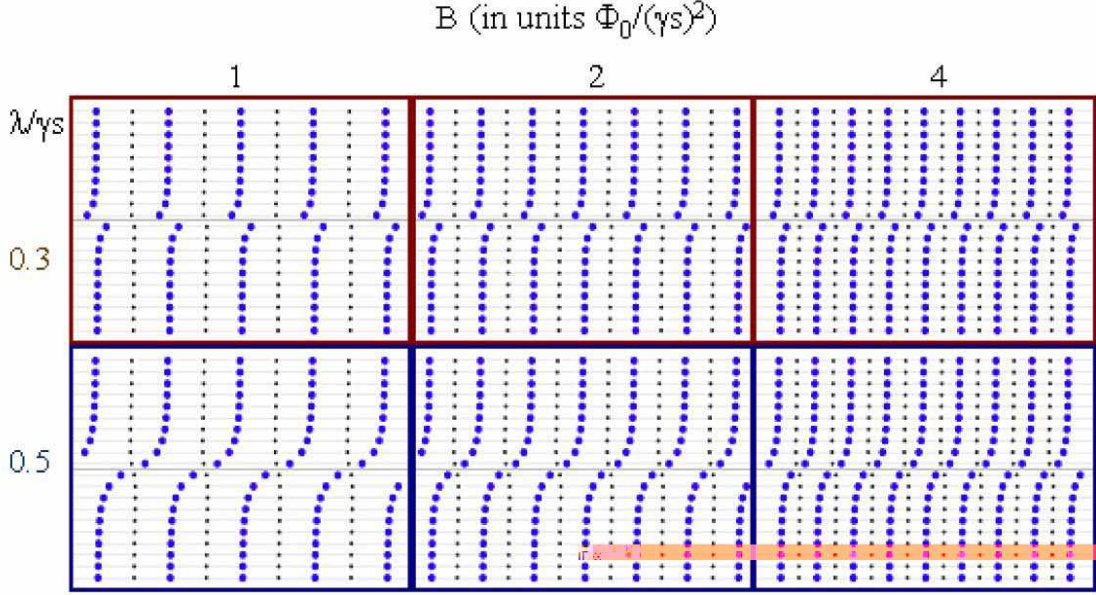


FIG. 7: Structure of the pancake-stacks row in the center of JV (big circles) and its neighboring row (small circles) for  $\lambda/\gamma s = 0.3$  and 0.5 and several values of the magnetic field. At  $\lambda/\gamma s = 0.5$  pancakes in the central row form lines smoothly transferring between two ideal lattice position (solitonlike structure).

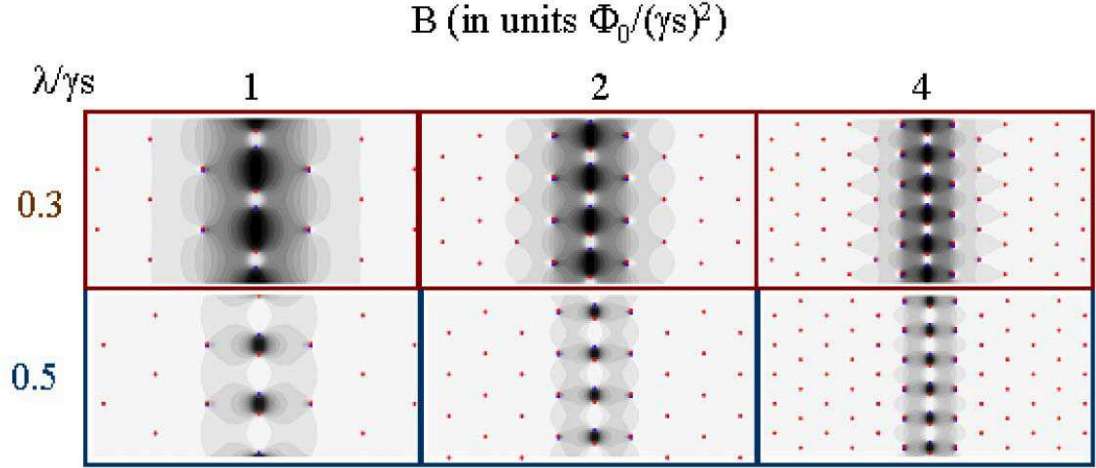


FIG. 8: Gray-level plots of cosine of interlayer phase difference between the two central layers of JV for  $\lambda/\gamma s = 0.3$  and 0.5 and different fields. For  $\lambda/\gamma s = 0.3$  the JV core covers roughly three pancake rows, while for  $\lambda/\gamma s = 0.5$  it shrinks to one pancake rows. In the second case the regions of suppressed Josephson energy are practically eliminated.

We also estimate the shear contribution to the periodic potential  $v_{\text{cage}}(v)$

$$v_{\text{shear}}(v) \approx \frac{2\lambda^2}{a^2} \frac{2(1 - \cos 2\pi v) \exp(-\sqrt{3}\pi)}{(1 + \exp(-\sqrt{3}\pi))^2} \\ \approx 0.017 \frac{\lambda^2}{a^2} (1 - \cos 2\pi v).$$

It occurs to be numerically small and only has to be taken into account when  $a$  becomes significantly smaller than

$\lambda$ .

It is important to note that the described model does not provide precise soliton structure. At distances  $z \gtrsim \lambda/\gamma$  displacements in other pancake rows become comparable with displacements in the central row. In fact, at distances  $z \gg \lambda/\gamma$  the displacements should cross over to the regime, described by the “effective phase stiffness” model (35). Precise description of the soliton structure is rather complicated and beyond the scope of this paper.

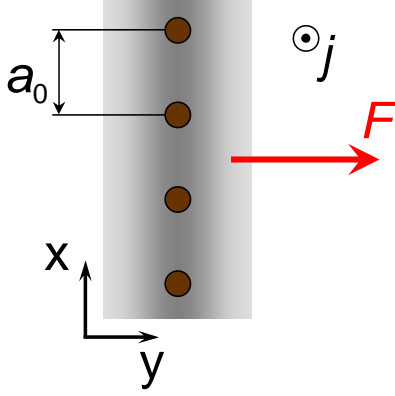


FIG. 9: Pinning of a Josephson vortex by a single pancake-stack row.

### III. PINNING OF JOSEPHSON VORTEX BY PANCAKE VORTICES

Dynamic properties of JVs can be probed either by applying transport current along the  $c$  direction or by studying  $ac$  susceptibility for magnetic field, polarized along the layers. Although there are numerous experimental indications that pancake vortices strongly impede motion of JVs,<sup>32,33,34</sup> no quantitative study (theoretical or experimental) has been done yet. In this section we consider a pinning force, which is necessary to apply to the JV to detach it from the pancake vortex crystal. We consider the simplest case of a dilute pancake lattice,  $a > \lambda$ , which allows us to neglect the influence of pancakes on the JV core, and small concentration of JVs, so that we can neglect influence of the JV lattice on the pancake crystal (e.g., formation of phase-separated states).

#### A. Pinning by a single pancake-stack row ( $a_0 > \gamma s$ )

We consider first the simplest case of an isolated pancake-stack row crossing JV (see Fig. 9) and estimate the force necessary to detach JV from this stack, assuming that its position is fixed. The consideration is based on the crossing energy of JV and isolated pancake stack, calculated in Sec. II B. Let us calculate first the force necessary to separate JV from an isolated pancake stack. Using Eq. (17) we obtain for the force acting on JV from the pancake stack located at distance  $y$  from the center of JV core

$$F_{\times} = -\frac{d}{dy} E_{\times}(y) \quad (65)$$

$$\approx \frac{\Phi_0^2}{4\pi^2 \gamma^3 s^2 \ln(\lambda/u_1(y))} A'_{\times} \left( \frac{y}{\gamma s} \right)$$

with  $A'_{\times}(\tilde{y}) \equiv dA_{\times}(\tilde{y})/d\tilde{y}$ . For the maximum force we obtain

$$F_{\times \max} \approx \frac{C_f \Phi_0^2}{4\pi^2 \gamma^3 s^2 \ln(\lambda/s\beta_f)}$$

with  $C_f = \max_{\tilde{y}} [A'_{\times}(\tilde{y})]$  and  $\beta_f \sim 1$ . Numerical calculation gives  $C_f \approx 1.4$  and the maximum is located at  $y_f \approx 0.52\gamma s$ . The critical current which detaches JV from the row of pancake stacks with the period  $a_0$  is given by

$$j_{Jp} = j_J \frac{C_f \lambda^2}{\gamma s a_0 \ln(\lambda/s\beta_f)}. \quad (66)$$

where  $j_J = c\Phi_0/(8\pi^2 \lambda_c^2 s)$  is the Josephson current. This expression is valid as long as the lattice period  $a_0$  is much larger than the Josephson length  $\gamma s$ . Otherwise interaction with several pancake rows has to be considered, which will be done in the next section.

#### B. Pinning by dilute pancake lattice ( $\lambda < a_0 < \gamma s$ )

When several pancake-stack rows fit inside the JV core (but still  $a_0 > \lambda$ ) interaction energy of JV per unit length with the pancake lattice,  $E_{Jl}(y)$ , can be calculated as a sum of crossing energies (17),

$$E_{Jl}(y) = \frac{1}{a_0} \sum_n E_{\times}(y - nb_0) \quad (67)$$

$$\approx -\frac{\Phi_0^2}{4\pi^2 \gamma^2 s a_0 \ln(\gamma s/\lambda)} \sum_{m=-\infty}^{\infty} A_{\times} \left( \frac{y - mb_0}{\gamma s} \right)$$

where  $b_0 = \sqrt{3}a_0/2$  is the distance between the PV rows. This expression has a logarithmic accuracy, i.e., we neglected a weak  $y$ -dependence under the logarithm and replaced the dimensionless function under the logarithm by its typical value. Using Fourier transform of  $E_{\times}(y)$ ,  $\tilde{E}_{\times}(p) = \int dy \exp(-ipy) E_{\times}(y)$ , we also represent  $E_{Jl}(y)$  as

$$E_{Jl}(y) = n_v \sum_{s=-\infty}^{\infty} \tilde{E}_{\times} \left( \frac{2\pi s}{b_0} \right) \exp \left( i \frac{2\pi m}{b_0} y \right)$$

In the case  $b_0 \ll \gamma s$  we can keep only  $m = 0, \pm 1$  terms in this sum,

$$E_{Jl}(y) \approx E_{Jl}(0) + 2n_v \tilde{E}_{\times} \left( \frac{2\pi}{b_0} \right) \cos \left( \frac{2\pi y}{b_0} \right)$$

Using interpolation formula (21) for  $A_{\times}(\tilde{y})$ , we obtain the asymptotics for  $b_0 < \gamma s$

$$E_{Jl}(y) - E_{Jl}(0) \approx -0.35 \frac{n_v \Phi_0^2}{\gamma \ln(\gamma s/\lambda)} \sqrt{\frac{\gamma s}{b_0}} \quad (68)$$

$$\times \cos \left( \frac{2\pi y}{b_0} \right) \exp \left( -5.82 \frac{\gamma s}{b_0} \right)$$



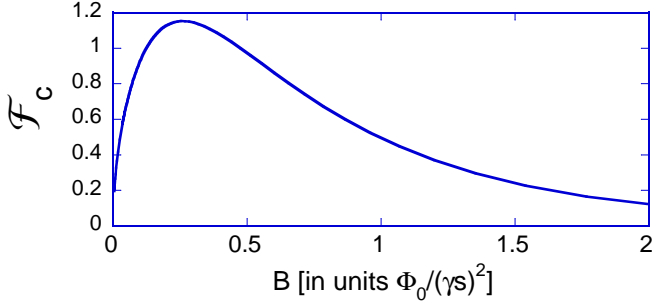


FIG. 10: The field dependence of the dimensionless pinning force of JV by dilute pancake vortex crystal

To compute the field dependence of the critical current, we represent the force acting on JV from the pancake lattice in the scaling form,

$$F_{Jpl}(y) \approx \frac{\sqrt{3}s\Phi_0^2}{(4\pi)^2(\gamma s)^4 \ln(\lambda/s)} \mathcal{F}\left(\frac{y}{\gamma s}, \frac{b_0}{\gamma s}\right),$$

with

$$\mathcal{F}(\tilde{y}, \tilde{b}_0) \equiv \frac{2}{b_0} \frac{d}{d\tilde{y}} \sum_j A_{\times}(\tilde{y} - j\tilde{b}_0).$$

The critical pinning current is given by

$$j_{Jpl} = j_J \frac{\sqrt{3}\lambda^2}{2(\gamma s)^2 \ln(\lambda/s)} \mathcal{F}_c(\tilde{b}_0) \quad (69)$$

with

$$\mathcal{F}_c(\tilde{b}_0) = \max_{\tilde{y}} [\mathcal{F}(\tilde{y}, \tilde{b}_0)]$$

Numerically calculated dependence of  $\mathcal{F}_c$  versus reduced field  $(\gamma s)^2 B / \Phi_0 \equiv \sqrt{3}/2\tilde{b}_0^2$ . Maximum  $\mathcal{F}_{c\max} \approx 1.15$  is achieved at  $B \approx 0.26\Phi_0/(\gamma s)^2$  ( $b_0 = 2.1\gamma s$ ). Therefore the maximum pinning current can be estimated as

$$j_{Jp\max} \approx j_J \frac{\lambda^2}{(\gamma s)^2 \ln(\lambda/s)} \quad (70)$$

For typical parameters of BSCCO this current is only 5-10 times smaller than the maximum Josephson current, i.e., it is actually rather large.

An exponential decay of the pinning energy (68) and force holds until the row separation  $b_0$  reaches  $\lambda$ . At larger fields one have to take into account shrinking of the vortex core. Because the number of pancake rows in the core is almost constant at high field, the exponential decay will saturate at a finite value  $\sim \exp(-C\gamma s/\lambda)$ .

#### IV. PANCAKE VORTICES AND VISCOSITY OF JOSEPHSON VORTEX

A sufficiently large  $c$  axis transport current will drive JVs. Two dynamic regimes are possible, depending on

the relation between the JV-pancake interaction and disorder-induced pancake pinning. Moving JVs either can drag the pancake lattice or they can move through the static pancake lattice. Slow dragging of pancake stacks by JVs at small  $c$  axis fields have been observed experimentally.<sup>17</sup> As the JV-pancake interaction force decays exponentially at high  $c$  axis fields in the case  $\lambda < \gamma s$ , one can expect that JVs will always move through the static pancake lattice at sufficiently high fields.

##### A. Dragging pancake lattice by Josephson vortices

When moving JVs drag the pancake lattice, one can obtain simple universal formulas for the JV viscosity coefficient and JV flux-flow resistivity. The effective viscosity coefficient per single JV is connected by a simple relation with the viscosity coefficient of pancake stack per unit length,  $\eta_v$ ,

$$B_x \eta_{JV} = B_z \eta_v.$$

Therefore, the JV flux-flow resistivity,  $\rho_{ff}^c(\mathbf{B}) = \Phi_0 B_x / (c^2 \eta_{JV})$ , is given by

$$\rho_{ff}^c(\mathbf{B}) = \frac{\Phi_0 B_x^2}{c^2 \eta_v B_z}. \quad (71)$$

As a consequence, we also obtain a simple relation between  $\rho_{ff}^c(\mathbf{B})$  and  $\rho_{ff}^{ab}(B_z)$

$$\rho_{ff}^c(\mathbf{B}) = \rho_{ff}^{ab}(B_z) \frac{B_x^2}{B_z^2}.$$

##### B. Josephson vortex moving through pancake lattice

Consider slow JV motion through the static pancake lattice. JV motion along the  $y$  direction with velocity  $V_y$  induces traveling pancake displacement field  $u_n(y - V_y t)$ . For slow motion,  $u_n(y)$  is just the static displacement field around JV. Contribution to the energy dissipation caused by these displacements is given by

$$\begin{aligned} W &\approx \eta_p n_v \sum_n \int d\mathbf{r} \dot{u}_n^2 \\ &= \eta_p \left[ n_v \sum_n \int d\mathbf{r} (\nabla_y u_n)^2 \right] V_y^2 \end{aligned}$$

where  $\eta_p$  is the pancake viscosity coefficient. Therefore the JV viscosity per unit length is given by

$$\eta_{JV} = \eta_p n_v \sum_n \int d\mathbf{r} (\nabla_y u_n)^2 \quad (72)$$

Using relation between the vortex phase and displacement field  $\nabla_y \phi_{vn} = 2\pi n_v u_n$  we obtain an estimate

$$n_v \sum_n \int dy (\nabla_y u_n)^2 \approx \frac{2.7\lambda^3 \sqrt{n_v}}{(\gamma s)^3} \left( \frac{\mathcal{C}}{\ln(r_{\text{cut}}/r_w)} \right)^{3/2}$$

with  $\mathcal{C} \equiv \langle \cos(\phi_{n+1} - \phi_n) \rangle < 1$ , and derive an approximate formula for the JV viscosity coefficient

$$\eta_{JV} \approx \eta_v \frac{s}{a} \frac{2.7\lambda^3}{(\gamma s)^3} \left( \frac{\mathcal{C}}{\ln \frac{r_{cut}}{r_w}} \right)^{3/2} \quad (73)$$

with  $\eta_v \equiv \eta_p/s$  is the viscosity of pancake stack per unit length. Because the JV viscosity  $\eta_{JV}$  is proportional to the pancake-stack viscosity  $\eta_v$ , there is a relation between the flux-flow resistivity of JVs ( $\rho_{ff}^c$ ) and the flux-flow resistivity of pancake vortices ( $\rho_{ff}^{ab}$ )

$$\frac{\rho_{ff}^c}{B_x} \approx \frac{\rho_{ff}^{ab}}{B_z} \frac{a}{s} \frac{0.37(\gamma s)^3}{\lambda^3} \left( \frac{\ln(r_{cut}/r_w)}{\mathcal{C}} \right)^{3/2} \quad (74)$$

If we use the Bardeen-Stephen formula for the in-plane flux-flow resistivity,  $\rho_{ff}^{ab} \approx \rho_{ab} B_z / H_{c2}$ , and an estimate for the  $c$  axis flux-flow resistivity at  $B_z = 0$ ,  $\rho_{ff}^{c0} \approx (16\gamma^3 s^2 B_x / \Phi_0) \rho_{ab}$ ,<sup>35</sup> we can also obtain relation between  $\rho_{ff}^c(B_z)$  and  $\rho_{ff}^{c0}$

$$\rho_{ff}^c \approx 0.15 \rho_{ff}^{c0} \frac{\xi^2 a}{\lambda^3} \left( \frac{\ln(r_{cut}/r_w)}{\mathcal{C}} \right)^{3/2} \quad (75)$$

From this estimate we can see that at  $a \sim \lambda$  the flux-flow resistivity for JVs slowly moving through the pancake lattice is about four order of magnitude (factor  $(\xi/\lambda)^2$ ) smaller than the flux-flow resistivity of free JVs. We see that even though the critical force becomes exponentially

small at high fields, pancakes still very strongly hinder mobility of JVs.

## V. ACKNOWLEDGEMENTS

I would like to thank V. Vlasko-Vlasov, T. Tamegai, A. Grigorenko, and S. Bending for fruitful discussions. I am very grateful to M. Dodgson for reading the manuscript and useful suggestions. This work was supported by the U. S. DOE, Office of Science, under contract # W-31-109-ENG-38.

## APPENDIX A: MAGNETIC INTERACTION BETWEEN PANCAKE ROWS

In this appendix we derive several useful representation for the magnetic interaction between pancake rows in different layers. The interaction energy between two pancakes in Fourier and real-space is given by Eq. (7). We will use also this interaction in the mixed representation

$$U_M(\mathbf{k}_\perp, n) \approx \frac{4\pi^2 J \delta_n}{k_\perp^2} - \frac{2\pi^2 s J}{\lambda^2 k_\perp^2} \frac{\exp\left(-ns\sqrt{\lambda^{-2} + k_\perp^2}\right)}{\sqrt{\lambda^{-2} + k_\perp^2}}$$

The interaction energy between the pancake rows per unit length is given by

$$\begin{aligned} U_{Mr}(x, y, n) &\equiv \frac{1}{a} \sum_m U_M(x - ma, y, n) \\ &= \frac{1}{a^2} \sum_l \int \frac{dk_y}{2\pi} U_M(k_x = \frac{2\pi l}{a}, k_y, n) \exp\left(i \frac{2\pi l}{a} x + i k_y y\right) \end{aligned}$$

From this equation we obtain the following integral representation for  $U_{Mr}(x, y, n)$

$$\begin{aligned} U_{Mr}(x, y, n) &= \frac{s\varepsilon_0}{a} \left[ -\left( \delta_n - \frac{s}{2\lambda} \exp\left(-\frac{s|n|}{\lambda}\right) \right) \ln \left[ 1 - 2 \cos \frac{2\pi x}{a} \exp\left(-\frac{2\pi|y|}{a}\right) + \exp\left(-\frac{4\pi|y|}{a}\right) \right] \right. \\ &\quad \left. + \frac{s}{a} \sum_l \int du \frac{\exp\left(i \frac{2\pi l}{a} x + i \sqrt{\lambda^{-2} + \left(\frac{2\pi l}{a}\right)^2} u s n - \sqrt{\lambda^{-2} + \left(\frac{2\pi l}{a}\right)^2} \sqrt{1 + u^2} |y|\right)}{\left(1 + \left(1 + \left(\frac{2\pi \lambda l}{a}\right)^2\right) u^2\right) \sqrt{1 + u^2}} \right] \end{aligned}$$

This representation can be used to derive large- $y$  asymptotics of  $U_{Mr}(x, y, n)$ ,

$$\begin{aligned} U_{Mr}(x, y, n) &\approx \frac{\pi J}{a} \left[ \left( \delta_n - \frac{s}{2\lambda} \exp\left(-\frac{s|n|}{\lambda}\right) \right) 2 \cos \frac{2\pi x}{a} \exp\left(-\frac{2\pi|y|}{a}\right) \right. \\ &\quad \left. + \frac{\sqrt{2\pi} s}{a} \frac{\exp\left(i \frac{2\pi x}{a} - \sqrt{\lambda^{-2} + \left(\frac{2\pi}{a}\right)^2} |y| - \frac{\sqrt{\lambda^{-2} + \left(\frac{2\pi}{a}\right)^2} (s n)^2}{2|y|}\right)}{\left(\lambda^{-2} + \left(\frac{2\pi}{a}\right)^2\right)^{1/4} \sqrt{|y|}} \right] \end{aligned}$$

at  $\sqrt{\lambda^{-2} + (2\pi/a)^2}|y| \gg 1$ . Therefore the interaction between the pancake rows decays exponentially at  $y, sn > \lambda, a$ . Interaction of pancake row with stack of rows is given by

$$\begin{aligned} U_{Ms}(x, y) &= 2 \sum_{n=1}^{\infty} U_{Mr}(x, y, n) \\ &= \frac{\pi J}{a} \ln \left[ 1 - 2 \cos\left(\frac{2\pi x}{a}\right) \exp\left(-\frac{2\pi y}{a}\right) + \exp\left(-\frac{4\pi y}{a}\right) \right] \\ &\quad + \frac{2\pi^2 J}{a} \sum_l \frac{\exp\left(i\frac{2\pi l}{a}x - \sqrt{\lambda^{-2} + \left(\frac{2\pi l}{a}\right)^2}y\right)}{\sqrt{(a/\lambda)^2 + (2\pi l)^2}} \end{aligned}$$

In particular, the potential created by pancakes belonging to the same row stack (“cage potential”) is given by

$$U_{\text{cage}} \equiv U_{Ms}(x, 0) = -\frac{4\pi^2 J}{a} \sum_{l=1}^{\infty} \cos\left(\frac{2\pi l}{a}x\right) \left( \frac{1}{2\pi l} - \frac{1}{\sqrt{(a/\lambda)^2 + (2\pi l)^2}} \right)$$

## APPENDIX B: LOCAL CONTRIBUTION TO JOSEPHSON ENERGY DUE TO MISMATCH OF PANCAKE ROWS IN NEIGHBORING LAYERS

We consider two pancake rows in neighboring layers with period  $a \ll \gamma s$  shifted at distance  $v$  with respect to each other in the direction of row ( $x$  axis). In zero order with respect to the Josephson coupling these rows produce the phase mismatch  $\varphi_v(x, y)$  between the layers,

$$\varphi_v(x, y) = \sum_m \left( \arctan \frac{x-m+v/2}{y} - \arctan \frac{x-m-v/2}{y} \right).$$

We measure all distances in units of the lattice constant  $a$ . The  $x$ -averaged phase mismatch is given by

$$\overline{\varphi}_v(y) = \pi v \operatorname{sgn}(y).$$

The total phase approaches  $\overline{\varphi}_v(y)$  at  $y \gtrsim 1/2\pi$ .

Separating  $\varphi_v(x, y)$  from the total phase, we can represent the Josephson energy as

$$\begin{aligned} \mathcal{F}_J &= E_J a^2 \int d^2 \mathbf{r} [1 - \cos(\varphi_v(x, y) + \varphi(x, y))] \\ &= E_J a^2 \int d^2 \mathbf{r} [1 - \cos(\overline{\varphi}_v(y) + \varphi(x, y))] + L_x \mathcal{E}_{Josc}(v, \varphi) \end{aligned}$$

where  $\varphi(x, y)$  is the smooth external phase and the local Josephson energy  $\mathcal{E}_{Josc}(v, \varphi)$  per unit length is defined as

$$\begin{aligned} \mathcal{E}_{Josc}(v, \varphi) &= -\frac{E_J a^2}{L_x} \int dx dy [\cos(\varphi + \varphi_v(x, y)) - \cos(\varphi + \overline{\varphi}_v(y))] \\ &= 2E_J a \cos(\varphi) \mathcal{J} \end{aligned} \tag{B1}$$

where

$$\mathcal{J}(v) \equiv \int_{-1/2}^{1/2} dx \int_0^{\infty} dy [\cos(\overline{\varphi}_v(y)) - \cos(\varphi_v(x, y))]. \tag{B2}$$

In  $\mathcal{E}_{Josc}(v, \varphi)$  we can neglect weak coordinate dependence of the external phase and replace it by a constant  $\varphi$ . At  $|v| < 1/2$  the ground state for fixed  $v$  corresponds to  $\varphi = 0$ , while at  $1/2 < |v| < 1$  the ground state corresponds to  $\varphi = \pi$ .  $\mathcal{E}_{Josc}(v, \varphi)$  has a symmetry property  $\mathcal{E}_{Josc}(1-v, \varphi) = -\mathcal{E}_{Josc}(v, \varphi)$ . The integral over  $y$  in  $\mathcal{J}(v)$  is converges at  $y \lesssim 1/2\pi$ . This allows us to consider a single row separately from other rows and neglect the coordinate dependence of the “external phase”  $\varphi$ .

Using the complex variable  $z = x + iy$  one can derive a useful expression for  $\varphi_v(x, y)$ :

$$\varphi_v(z) = \text{Im} \left( \ln \prod_m \frac{z - m - v/2}{z - m + v/2} \right) = \text{Im} \left( \ln \frac{\sin(\pi(z - v/2))}{\sin(\pi(z + v/2))} \right).$$

Going back to the  $(x, y)$  representation, we obtain

$$\varphi_v(x, y) = \arctan \frac{\tan(\pi(x + v/2))}{\tanh \pi y} - \arctan \frac{\tan(\pi(x - v/2))}{\tanh \pi y}$$

and

$$\cos \varphi_v(x, y) = \frac{\cosh 2\pi y \cos \pi v - \cos 2\pi x}{\sqrt{(\cosh 2\pi y - \cos 2\pi x \cos \pi v)^2 - (\sin 2\pi x \sin \pi v)^2}}.$$

Integral (B2) can now be represented as

$$\mathcal{J}(v) = \int_{-1/2}^{1/2} dx \int_0^\infty dy \left[ \cos(\pi v) - \frac{\cosh 2\pi y \cos \pi v - \cos 2\pi x}{\sqrt{(\cosh 2\pi y - \cos 2\pi x \cos \pi v)^2 - (\sin 2\pi x \sin \pi v)^2}} \right]$$

We obtain an approximate analytical result at small  $v$ ,  $v \ll 1$ . Simple expansion with respect to  $v$  produces logarithmically diverging integral. To handle this problem we introduce the intermediate scale  $y_0$ ,  $v \ll y_0 \ll 1$ , and split integral  $\mathcal{J}$  into contribution coming from  $y > y_0$  ( $\mathcal{J}_>$ ) and  $y < y_0$  ( $\mathcal{J}_<$ ). At  $y > y_0$  we use small- $v$  expansion and obtain

$$\begin{aligned} \mathcal{J}_> &= (\pi v)^2 \int_{y_0}^\infty dy \int_0^{1/2} dx \left( -1 + \frac{\sinh^2 2\pi y}{(\cosh 2\pi y - \cos 2\pi x)^2} \right) \\ &= \frac{(\pi v)^2}{2} \int_{y_0}^\infty dy \frac{\exp(-2\pi y)}{\sinh 2\pi y} \\ &\approx \frac{\pi v^2}{4} \ln \frac{1}{4\pi y_0}. \end{aligned}$$

In region  $y < y_0$  we can expand all trigonometric functions and obtain the integral

$$\begin{aligned} \mathcal{J}_< &\approx 2 \int_0^{y_0} dy \int_0^{1/2} dx \left[ 1 - \frac{4(x^2 + y^2) - v^2}{\sqrt{(4(x^2 + y^2) + v^2)^2 - (4xy)^2}} \right] \\ &= \frac{v^2}{2} \int_0^{2y_0/v} d\tilde{y} \int_0^{1/v} d\tilde{x} \left[ 1 - \frac{\tilde{x}^2 + \tilde{y}^2 - 1}{\sqrt{(\tilde{x}^2 + \tilde{y}^2 - 1)^2 + 4\tilde{y}^2}} \right] \end{aligned}$$

with  $\tilde{y} = 2y/v$  and  $\tilde{x} = 2x/v$ . Because we only interested in the main logarithmic term, we can extend integration over  $\tilde{x}$  up to  $\infty$ . The obtained integral can be evaluated as

$$\mathcal{J}_< \approx \frac{\pi}{4} v^2 \left( \ln \frac{y_0}{v} + 1.58 \right)$$

Adding  $\mathcal{J}_>$  and  $\mathcal{J}_<$ , we obtain

$$\mathcal{J}(v) \approx \frac{\pi}{4} v^2 \left( \ln \frac{1}{v} - 0.95 \right) \quad (\text{B3})$$

and

$$E_{Josc}(v, \varphi) \approx \frac{\pi}{2} E_{Ja} \cos(\varphi) v^2 \left( \ln \frac{1}{v} - 0.95 \right) \quad (\text{B4})$$

We also calculated function  $\mathcal{J}(v)$  numerically for the whole range  $0 < v < 1/2$ . The result is shown in Fig. 11 and is described by approximate interpolation formula

$$\begin{aligned} \mathcal{J}(v) &\approx \frac{1 - \cos \pi v}{4\pi} \\ &\times \left( \ln \frac{1}{1 - \cos \pi v} - 0.379 \cos \pi v + 0.076 \cos^2 \pi v \right) \end{aligned} \quad (\text{B5})$$

This result was used in numerical calculations of the JV core structure.

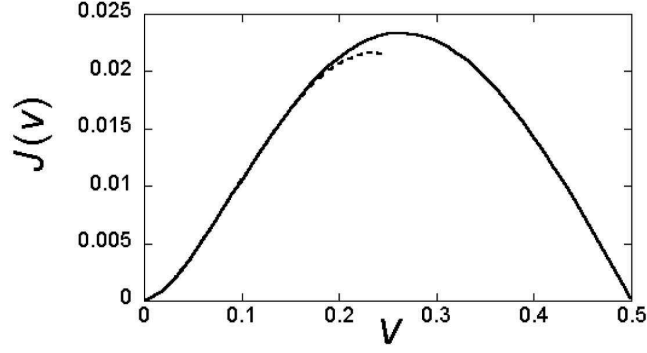


FIG. 11: Dimensionless function  $\mathcal{J}(v)$  which determines the local Josephson energy. Dashed line is small- $v$  asymptotics (B3).

### APPENDIX C: CONTRIBUTION TO JV ENERGY COMING FROM LOCAL JOSEPHSON TERM AT $\gamma \gg \lambda/s$

energy is given by

In the limit of very weak coupling the correction to reduced JV energy (57) coming from the local Josephson

$$\delta\mathcal{E}_{JV} \approx \frac{\pi\sqrt{3}}{4\sqrt{1+B_z/B_\lambda}} \sum_{n=-\infty}^{\infty} \int_{-\infty}^{\infty} d\tilde{y} (v_{n+1} - v_n)^2 \ln \frac{0.39}{|v_{n+1} - v_n|} \cos(\phi_{n+1} - \phi_n) \quad (C1)$$

with  $\tilde{y} = y/\lambda_J = \sqrt{1+B_z/B_\lambda} y/\gamma s$ . We will focus only on the regime  $B_z \gg B_\lambda$ , where this correction can be noticeable. In this regime reduced row displacements are connected with phase gradient by relation

$$v_n(y) \approx \frac{b}{2\pi\lambda_J} \tilde{\nabla}_y \phi_n$$

and the correction reduces to

$$\delta\mathcal{E}_{JV} \approx \frac{\sqrt{B_z/B_\lambda}}{8\pi n_v (\gamma s)^2} \sum_n \int d\tilde{y} \left( \tilde{\nabla}_y \phi_{n+1} - \tilde{\nabla}_y \phi_n \right)^2 \ln \left[ \frac{2.83 \gamma s \sqrt{B_\lambda/B_z}}{a |\tilde{\nabla}_y \phi_{n+1} - \tilde{\nabla}_y \phi_n|} \right] \cos(\phi_{n+1} - \phi_n). \quad (C2)$$

Using numerical estimates

$$\begin{aligned} \sum_{n=-\infty}^{\infty} \int_{-\infty}^{\infty} d\tilde{y} \cos(\phi_{n+1} - \phi_n) \left( \tilde{\nabla}_y \phi_{n+1} - \tilde{\nabla}_y \phi_n \right)^2 &\approx -2.4 \\ \sum_{n=-\infty}^{\infty} \int_{-\infty}^{\infty} d\tilde{y} \cos(\phi_{n+1} - \phi_n) \left( \tilde{\nabla}_y \phi_{n+1} - \tilde{\nabla}_y \phi_n \right)^2 \ln \frac{1}{|\tilde{\nabla}_y \phi_{n+1} - \tilde{\nabla}_y \phi_n|} &\approx 4.7 \end{aligned}$$

obtained with the JV phase  $\phi_n(\tilde{y})$  (14), we obtain

$$\delta\mathcal{E}_{JV} \approx -\pi \sqrt{\frac{B_\lambda}{B_z}} \frac{0.38\lambda^2}{(\gamma s)^2 \ln(a/r_w)} \ln \left[ \frac{0.1 \gamma s}{\lambda} \sqrt{\ln \frac{a}{r_w}} \right]. \quad (C3)$$

As we can see, the correction is smaller than the reduced JV energy at  $B_z \gg B_\lambda$ ,  $\mathcal{E}_{JV} \approx \pi \sqrt{B_\lambda/B_z} \ln(a/s)$ , by the factor  $\sim \lambda^2/(\gamma s)^2$ .

- <sup>1</sup> A. I. Buzdin and D. Feinberg, J. Phys. (Paris) **51**, 1971 (1990); S. N. Artemenko and A. N. Kruglov, Phys. Lett. A **143** 485 (1990); J. R. Clem, Phys. Rev. B **43**, 7837 (1991).
- <sup>2</sup> L. N. Bulaevskii, Zh. Eksp. Teor. Fiz. **64**, 2241 (1973) [Sov. Phys. JETP **37**, 1133 (1973)].
- <sup>3</sup> J. R. Clem and M. W. Coffey, Phys. Rev. B, **42**, 6209 (1990); J. R. Clem, M. W. Coffey, and Z. Hao, Phys. Rev. B **44**, 2732 (1991).
- <sup>4</sup> A. E. Koshelev, Phys. Rev. B **48**, 1180 (1993).
- <sup>5</sup> L. N. Bulaevskii, M. Ledvij, and V. G. Kogan, Phys. Rev. B **46**, 366 (1992); M. Benkraouda and M. Ledvij, Phys. Rev. B **51**, 6123 (1995).
- <sup>6</sup> A. E. Koshelev, Phys. Rev. Lett. **83**, 187 (1999).
- <sup>7</sup> D. Feinberg and A. M. Ettouhami, Int. J. Mod. Phys. B **7**, 2085 (1993).
- <sup>8</sup> A. I. Buzdin and A. Yu. Simonov, JETP Lett. **51**, 191 (1990); A. M. Grishin, A. Y. Martynovich, and S. V. Yampolskii, Sov. Phys. JETP **70**, 1089 (1990); B. I. Ivlev and N. B. Kopnin, Phys. Rev. B **44**, 2747 (1991); W. A. M. Morgado, M. M. Doria, and G. Carneiro, Physica C, **349**, 196 (2001).
- <sup>9</sup> L. L. Daemen, L. J. Campbell, A. Yu. Simonov, and V. G. Kogan Phys. Rev. Lett. **70**, 2948 (1993); A. Sudbø, E. H. Brandt, and D. A. Huse Phys. Rev. Lett. **71**, 1451 (1993); E. Sardella, Physica C **257**, 231 (1997).
- <sup>10</sup> Direction of magnetic induction  $\mathbf{B}$  almost never coincides with direction of external magnetic field  $\mathbf{H}_{ext}$ . The relation between  $\mathbf{B}$  and  $\mathbf{H}_{ext}$  depends on the shape of sample and constitutes a separate problem.
- <sup>11</sup> S. E. Savel'ev, J. Mirkovic, K. Kadowaki, Phys. Rev. B **64**, 094521 (2001).
- <sup>12</sup> B. Schmidt, M. Konczykowski, N. Morozov, and E. Zeldov, Phys. Rev. B **55**, R8705 (1997).
- <sup>13</sup> S. Ooi, T. Shibauchi, N. Okuda, and T. Tamegai, Phys. Rev. Lett. **82**, 4308 (1999).
- <sup>14</sup> D. A. Huse, Phys. Rev. B **46**, 8621 (1992).
- <sup>15</sup> C. A. Bolle, P. L. Gammel, D. G. Grier, C. A. Murray, D. J. Bishop, D. B. Mitzi, and A. Kapitulnik, Phys. Rev. Lett. **66**, 112 (1991).
- <sup>16</sup> I. V. Grigorieva, J. W. Steeds, G. Balakrishnan, and D. M. Paul, Phys. Rev. B **51**, 3765 (1995).
- <sup>17</sup> A. Grigorenko, S. Bending, T. Tamegai, S. Ooi, and M. Henini, Nature **414**, 728 (2001).
- <sup>18</sup> T. Matsuda, O. Kamimura, H. Kasai, K. Harada, T. Yoshida, T. Akashi, A. Tonomura, Y. Nakayama, J. Shimoyama, K. Kishio, T. Hanaguri, and K. Kitazawa, Science, **294**, 2136 (2001).
- <sup>19</sup> V. K. Vlasko-Vlasov, A. E. Koshelev, U. Welp, G. W. Crabtree, and K. Kadowaki, Phys. Rev. B **66**, 014523 (2002).
- <sup>20</sup> M. Tokunaga, M. Kobayashi, Y. Tokunaga, and T. Tamegai, Phys. Rev. B **66**, 060507 (2002).
- <sup>21</sup> M. J. W. Dodgson, Phys. Rev. B **66**, 014509 (2002).
- <sup>22</sup> A. Buzdin and I. Baladié, Phys. Rev. Lett. **88**, 147002 (2002).
- <sup>23</sup> M. Konczykowski, C. J. van der Beek, M. V. Indenbom, E. Zeldov, Physica C, **341**, 1213 (2000).
- <sup>24</sup> J. Mirkovic, S. E. Savelev, E. Sugahara, and K. Kadowaki, Phys. Rev. Lett. **86**, 886 (2001).
- <sup>25</sup> S. Ooi, T. Shibauchi, K. Itaka, N. Okuda, and T. Tamegai, Phys. Rev. B **63**, 020501(R) (2001).
- <sup>26</sup> M. Tokunaga, M. Kishi, N. Kameda, K. Itaka, and T. Tamegai, Phys. Rev. B **66**, 220501(R) (2002).
- <sup>27</sup> The more quantitative expression for  $U_{44}(\mathbf{k})$ , which accounts for thermal softening, can be obtained using the self-consistent harmonic approximation. At high fields and  $k_z > r_w^{-1}$  it gives  $U_{44}(\mathbf{k}) \approx \frac{n_v \epsilon_0}{2\lambda^2} \ln \left( 0.5 + \frac{0.13 a^2}{r_w^2} \right)$ , see A. E. Koshelev and L. N. Bulaevskii Physica C, **341-348**, 1503 (2000).
- <sup>28</sup> The formula (B12) for the JV phase in Ref. 4 for phase distribution  $\phi_n$  was written incorrectly. Eq. (14) gives correct phase distribution, which was actually used in all numerical calculations and is plotted in Fig. 8 of Ref. 4.
- <sup>29</sup> A. E. Koshelev and P. H. Kes, Phys. Rev. B **48**, 6539 (1993).
- <sup>30</sup> T. R. Goldin and B. Horovitz, Phys. Rev. B **58**, 9524 (1998).
- <sup>31</sup> The identical factor  $1 + B_z/B_\lambda$  appears also in the renormalization of defect energy by the pancake vortex crystal and have precisely the same physical origin, see M. J. W. Dodgson, V. B. Geshkenbein, and G. Blatter, Phys. Rev. Lett. **83**, 5358 (1999).
- <sup>32</sup> Yu. Latyshev and A. Volkov, Physica C, **182**, 47 (1991).
- <sup>33</sup> H. Enriquez, N. Bontemps, P. Fournier, A. Kapitulnik, A. Maignan, and A. Ruyter, Phys. Rev. B, **53**, R14757 (1996).
- <sup>34</sup> G. Hechtfisher, R. Kleiner, K. Schlenga, W. Walkenhorst, P. Müller, and H. L. Johnson, Phys. Rev. B **55**, 14638 (1997).
- <sup>35</sup> A. E. Koshelev, Phys. Rev. B **62**, R3616 (2000).